

# Robust modeling and inference of disease transmission using error-prone data with application to SARS-CoV-2

Jiasheng Shi

Department of Biostatistics, Epidemiology and Informatics,  
University of Pennsylvania, Philadelphia, PA, USA

Jeffrey S. Morris

Department of Biostatistics, Epidemiology and Informatics,  
University of Pennsylvania, Philadelphia, PA, USA

David M. Rubin

PolicyLab, Children's Hospital of Philadelphia, Philadelphia, PA, USA

and

Jing Huang

Department of Biostatistics, Epidemiology and Informatics,  
University of Pennsylvania, Philadelphia, PA, USA

---

\*Correspondence to: Jing Huang, Department of Biostatistics, Epidemiology, and Informatics, Perelman School of Medicine, University of Pennsylvania, 625 Blockley Hall, 423 Guardian Drive, Philadelphia, PA 19104, USA. E-mail: jing14@pennmedicine.upenn.edu. TEL: (215) 573-7398

**Authors' Footnote:** Jiasheng Shi is Post Doctoral Fellow, Department of Biostatistics, Epidemiology, and Informatics, Perelman School of Medicine, University of Pennsylvania, Philadelphia, PA 19104, USA ([Jiasheng.Shi@Pennmedicine.upenn.edu](mailto:Jiasheng.Shi@Pennmedicine.upenn.edu)). Jeffrey S. Morris is Professor and Division Director, Department of Biostatistics, Epidemiology, and Informatics, Perelman School of Medicine, University of Pennsylvania, Philadelphia, PA 19104, USA ([Jeffrey.Morris@pennmedicine.upenn.edu](mailto:Jeffrey.Morris@pennmedicine.upenn.edu)). David M. Rubin is Professor and Director, PolicyLab, Children's Hospital of Philadelphia, Philadelphia, PA 19104, USA ([rubin@chop.edu](mailto:rubin@chop.edu)). Jing Huang is Assistant Professor, Department of Biostatistics, Epidemiology, and Informatics, Perelman School of Medicine, University of Pennsylvania, Philadelphia, PA 19104, USA ([Jing14@Pennmedicine.upenn.edu](mailto:Jing14@Pennmedicine.upenn.edu)).

## Abstract

Modeling disease transmission is important yet challenging during a pandemic. It is not only critical to study the generative nature of a virus and understand the dynamics of transmission that vary by time and location but also crucial to provide accurate estimates that are robust to the data errors and model assumptions due to limited understanding of the new virus. We bridged the epidemiology of pathogens and statistical techniques to propose a hybrid statistical-epidemiological model so that the model is generative in nature yet utilizes statistics to model the effect of covariates (e.g., time and interventions), stochastic dependence, and uncertainty of data. Our model considers disease case counts as random variables and imposes moment assumptions on the number of secondary cases of existing infected individuals at the time since infection. Under the quasi-score framework, we built an “observation-driven model” to model the serial dependence and estimate the effect of covariates, with the capability of accounting for errors in the data. We proposed an online estimator and an effective iterative algorithm to estimate the instantaneous reproduction number and covariate effects, which provide a close monitoring and dynamic forecasting of disease transmission under different conditions to support policymaking at the community level.

*Keywords:* *instantaneous reproduction number; observation-driven model; online estimator; quasi-score method; time-since-infection model*

# 1 Introduction

The onset of the global pandemic of coronavirus disease 2019 (COVID-19), caused by the novel severe acute respiratory syndrome coronavirus 2 (SARS-CoV-2), elevated the importance of modeling and inference of disease transmission. However, both the classic epidemiological framework and modern statistical models for infectious diseases face challenges for modeling transmission and supporting decision making during a pandemic.

First, the classic mathematical epidemiological models provide a basic infrastructure and interpretable estimates to understand the generative nature of a virus but have limited ability to answer extended questions beyond virus generation that are important for decision making. In epidemiological studies, the transmission of an infectious pathogen is estimated by the reproduction number,  $R$ , which represents the average number of people that will be infected by an individual who has the infection. Many mathematical epidemiological models have been proposed to estimate  $R$ , including models to estimate the static basic reproduction number  $R_0$  and the time-varying reproduction number. The  $R_0$  is a constant representing the average spread potential of the virus over a long period of time in a fully susceptible population, while the time-varying reproduction number measures the disease transmission at a specific time, which is more useful for understanding the dynamics of transmission during a pandemic. The time-varying reproduction number has multiple definitions based on different epidemiological models, including the effective reproduction number ([Wallinga and Teunis, 2004](#)), instantaneous reproduction number ([Fraser, 2007](#)), case reproduction number ([Fraser, 2007](#)), and the reproduction number of time-dependent susceptible-infected-recovered (SIR) Models ([Chen et al., 2020](#)), ([Song et al., 2020](#)), ([Boatto et al., 2018](#)). Most of these existing definitions are based on two basic model frameworks, the SIR ordinary differential equations model and the time-since-infection (TSI) model,

both of which are originated from the classic paper of [Kermack and McKendrick \(1927\)](#) and are known as “the Kermack-McKendrick models”.

During the COVID-19 pandemic, many models were introduced purely based on these classic epidemiological models to estimate the transmission of SARS-CoV-2 ([Wang et al., 2020](#); [Pan, Liu, Wang, Guo, Hao, Wang, Huang, He, Yu, Lin et al., 2020](#); [Tian et al., 2020](#); [Zhou et al., 2020](#)). These models provided estimates of reproduction numbers but had limited ability to evaluate the effect of control policies or the impact of risk factors. Specifically, the evolution of a new outbreak is driven by multiple factors that almost certainly vary by time and location, including socio-behavioral, environmental and biological factors ([Rubin et al., 2020](#)). Policymakers also need to vary their control measures based on the current status of the outbreak as well as time-varying/invariant local factors. These control measures may also have unintended consequences on global economy and human health. To optimize the decision making, it is important to evaluate the benefit and harm of control strategies adjusting for local factors and many other variables.

On the other hand, modern statistical or computational models, while possess a great flexibility to capture the complex shape of disease curve, e.g. time series models ([IHME COVID-19 forecasting team, 2020](#); [Pan, Shen and Hu, 2020](#)) and machine learning models for curve data ([Dayan et al., 2021](#); [Punn et al., 2020](#); [Ardabili et al., 2020](#)), also have limited use to support decision making due to the lack of epidemiological interpretations of parameters. Therefore, the study results from these models may not be directly used to support decision making either.

In addition to the limitation of models, poor data quality collected during a pandemic can also bias study results and mislead decision making for both the epidemiological and statistical models. Data collection is labor intensive and, for health departments, it can

be challenging to stay on top of the numbers across counties due to the lack of shared standards for reporting data, different definitions of diseased individual, varying testing strategies and limited capacity of testing incident cases ([Costa-Santos et al., 2021](#); [Sáez et al., 2021](#)). Moreover, models that rely on strong statistical assumptions could further suffer from model mis-specification or failure to include important variables. To better support decision making, it is urgent to build a model with interpretable and accurate estimates that characterize the dynamics of transmission and, more importantly, robust to errors in data and model assumptions.

Motivated from these challenges, we propose a model to bridge the epidemiological modeling of pathogens and flexibility of statistical modeling, and utilize statistical techniques to improve the model robustness. Our proposed model combines the benefits of both the classic epidemiological models and modern statistical models, so that the model is generative in nature yet flexible to model the stochastic dependence of daily transmission, effect of local factors, and errors of data. Specifically, our model forms a two-layer hierarchical structure. On the first layer, we characterize the disease transmission using the instantaneous reproduction number of the TSI model, denoted as  $\{R_t\}_{t \geq 0}$ , by assuming the infectiousness of a diseased individual depends on the time since infection. On the second layer, we build a time series regression model to model correlation between daily transmission and characterize the impact of control measures and local factors. Under a quasi-score framework, we utilize an error term to correct bias due to errors in the data and model mis-specification. To fully characterize the real time impact of local area factors on disease transmission, we proposed an online estimator for  $R_t$ , and constructed an effective iterative algorithm to simultaneously estimate  $R_t$  and effects of covariates. A regression model based on the TSI model was recently proposed by [Quick et al. \(2021\)](#). The contribution

of our work is different from theirs. [Quick et al. \(2021\)](#) tackled case under-ascertainment using additional data resources, e.g. serological surveys and testing metrics, which might not be available in some regions or at the beginning of a pandemic. In our model, the bias due to errors in the data is handled using an error term while data used in our model, e.g. the case incidence data and geographical variables, are largely available across the country during a pandemic. In addition, we focus on building a robust estimation and predictive procedure under fewer model assumptions.

The rest of the paper is organized as follows. We introduce the TSI model and notations in Section 2, followed by description of the proposed model in Section 3. In section 4, we present the asymptotic results and property of estimating procedure under a special case. We show a robust performance of our method in simulation in Section 5, an application to COVID-19 data in Section 6 and a miscellany of discussions in Section 7. Proofs for theoretical properties are shown in the supplementary material.

## 2 The time-since-infection Model and Generative Nature of a Virus

The TSI model assumes that infectiousness of an infected individual depends on the time since infection. Let  $\beta(t, s)$  denote the effective contact rate at time  $t$  between susceptible individuals and an infected individual who was infected  $s$  time ago, indicating the number of secondary cases that an infected individual can generate at time  $t$ . The total number of new cases in the population infected at time  $t$ , denoted as  $I_t$ , can be written as a function of the effective contact rate at time  $t$  and the number of all existing cases that were infected before time  $t$ , i.e.  $\mathbb{E}(I_t) = \mathbb{E} \int_0^t \beta(t, s) I_{t-s} ds$ . The instantaneous reproduction number,  $R_t$ , which

measures how many secondary infections can be generated from someone infected at time  $t$  could expect to infect if conditions remain unchanged, is defined as  $R_t = \int_0^t \beta(t, s)ds$ .  $\beta(t, s)$  varies as the time since infection  $s$  changes, which typically reflects the change of pathogen shedding since infection. In microbiology, it has been found that pathogen shedding is an important determinant for disease transmission (Cevik et al., 2021). If we assume that the change of  $\beta(t, s)$  as a function of time since infection  $s$  is independent of calendar time  $t$ , then the  $\beta(t, s)$  can be decomposed as  $\beta(t, s) = R_t \omega_s$ . Here  $\omega_s$  is the infectiousness function, measuring infectiousness at the time since infection  $s$ , with  $\int_0^\infty \omega_s ds = 1$ , and  $\omega_s = 0$  for  $s = 0$  and  $s \geq \eta$  with  $\eta$  being the time to recovery since infection. Figure 1 shows an example of the infectiousness function at day  $s$  since infection,  $\omega_s$ , approximated using the density function of a gamma distribution with shape and rate parameters equals to 2.5 and 0.255 respectively. The shape of this  $\omega_s$  over time assumes that the infectiousness of an infected individual increases during the first 7 days since infection as viral loads increase soon after infection and then gradually decrease as the individual proceeds to recovery around 21 days after infection.

Based on these assumptions, we have  $\mathbb{E}(I_t) = R_t \mathbb{E} \int_0^t \omega_s I_{t-s} ds$ . In practice, we can discretize time to be equally spaced time points, so

$$E(I_t | I_0, \dots, I_{t-1}) = R_t \sum_{s=1}^t I_{t-s} \omega_s \triangleq R_t \Lambda_t, \quad (2.1)$$

where  $\sum_{s=0}^\infty \omega_s = 1$ . To estimate  $R_t$  and  $\omega_s$ , it is natural to assume a distribution assumption for  $I_t$  based on (2.1). For example, Cori et al. (2013) assumed a Poisson distribution, which is equivalent to model  $\{I_t, t \geq 0\}$  using a Poisson process. The model was used to study the epidemic of Ebola virus disease in west Africa (WHO Ebola Response Team, 2014). Recently, TSI model with an embedded regression structure is used to study

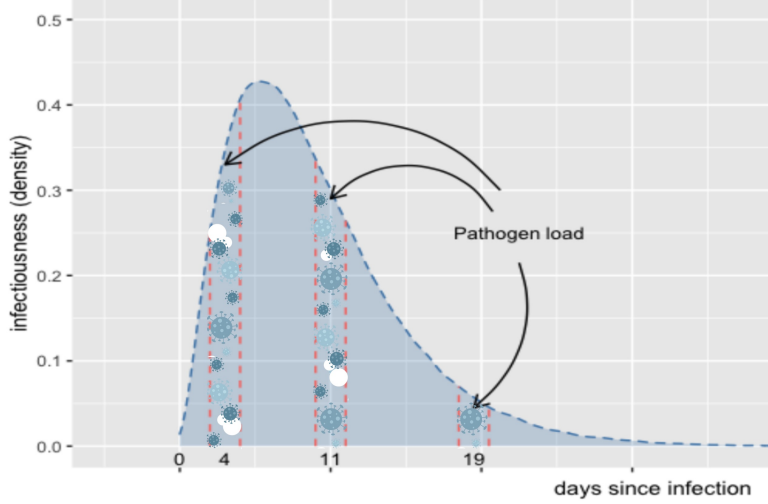


Figure 1: An example of the infectiousness function at day  $s$  since infection,  $\omega_s$ , approximated using the density function of a gamma distribution with shape and rate parameters equals to 2.5 and 0.255 respectively. The above  $\omega_s$  assumes that the infectiousness of an infected individual increases during the first 7 days since infection as viral loads increase soon after infection and then gradually decrease as the individual proceeds to recovery around 21 days after infection.

COVID-19 ([Quick et al., 2021](#)).

### 3 The proposed Quasi-Score approach

Now, we introduce a quasi-score method based on the TSI model, which relaxes the distribution assumptions and allows estimation of covariates effects on disease transmission with the capability of accounting for errors in the data.

### 3.1 The proposed model

To relax distributional assumptions, we assume moment constraints on the number of incidence cases at time  $t$  given observed incidence cases before time  $t$  as follows.

$$\mu_t \triangleq \mathbb{E}(I_t | \mathcal{F}_{t-1}) = \mathbb{E}(R_t | \mathcal{F}_{t-1}) \Lambda_t, \quad \nu_t \triangleq \text{Var}(I_t | \mathcal{F}_{t-1}) = g(\mu_t) \cdot \phi, \quad (3.1)$$

where  $\phi$  is a dispersion parameter and  $g(\cdot)$  is assumed to be a known variance function in the main manuscript. For a more general scenario where  $g(\cdot)$  is unknown, we provide the estimation and discussion in the supplementary material. When  $R_t \in \mathcal{F}_{t-1}$ ,  $\mu_t = R_t \Lambda_t$ . To estimate  $R_t$ ,  $t = 1, \dots, N$ , and investigate the impacts of local area factors (or covariates), e.g., temperature, social distancing measures and population density, on disease transmission, we adopt a time series model such that

$$h(R_t) = X_t^T \beta + \sum_{i=1}^q \theta_i f_i(D_{1,t}, D_{2,t}, D_{3,t}) + \epsilon_t. \quad (3.2)$$

where  $X_t^T = (1, Z_t^T) \in \mathcal{M}_{p \times 1}$  is the vector of intercept and covariates,  $Z_t$ , at time  $t$  and  $\theta_i \geq 0$  for  $1 \leq i \leq q$ . Here  $h(\cdot)$  and  $f_i(\cdot)$  represent a known link function and functions of past data respectively, and

$$D_{1,t} = \{X_j\}_{0 \leq j \leq t}, \quad D_{2,t} = \{I_j\}_{0 \leq j \leq t-1}, \quad D_{3,t} = \{R_j\}_{0 \leq j \leq t-1}, \quad \mathcal{F}_{t-1} = \sigma(D_{1,t} \cup D_{2,t}).$$

The  $\epsilon_t$  can be viewed as a measurement error term of  $R_t$ , although  $R_t$  is not directly observed. Such an error can be due to errors in the observed data or model mis-specification. Alternatively, the  $\epsilon_t$  can also be considered as a “random effect” for each day which captures the variation of  $R_t$  that are not explained by the time series structure and the unobserved data in equation (3.2).

Therefore, the proposed model decomposes the serial dependency of incidence cases into two parts: equation (3.1) models the serial dependency that is due to the generative

nature of disease transmission given  $R_t$ , and equation (3.2) models the serial dependency that is due to the dependency of  $R_t$  between neighboring time points that can be explained by covariates and time series structures. Conceptually, the proposed model is similar to a recurrent neural network as shown in Figure 2.

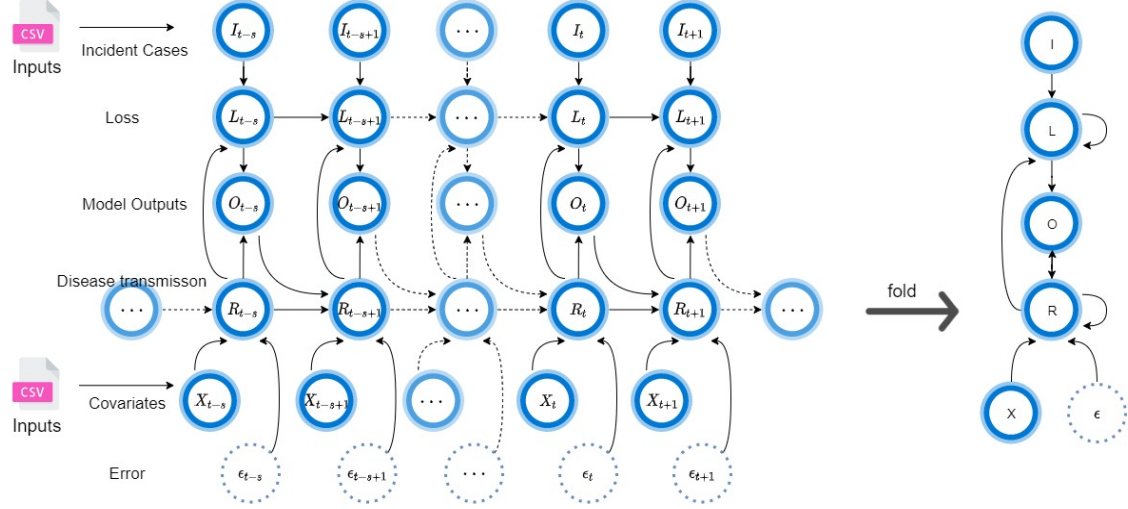


Figure 2: Workflow of the proposed dynamical systems described by model (3.1) and (3.2), illustrated as a recurrent neural network's computational graph. Combine the information of incident cases ( $I_t$ ) and daily covariates ( $X_t$ ), the proposed model constructs and solves an estimating function which is similar to minimizing a loss function to estimate parameters, e.g., covariates effects, and the time series dependency of the instantaneous reproduction number ( $R_t$ ).

In practice, a convenient special case of (3.2) is a non-stationary log-transmission model which assumes

$$\log(R_t) = \phi_0 + Z_t^T \beta + \sum_{i=1}^q \theta_i \log(R_{t-i}) + \epsilon_t, \quad \text{for } t \geq q > 0, \quad \theta_i \geq 0, \quad \text{and } \|\theta\|_1 < 1 \quad (3.3)$$

and  $\mu_t = \nu_t$ , where an  $AR(q)$  model is used to model the time series dependency and

the non-stationary of  $R_t$  is due to the variation of exogenous covariates. We impose the regularity condition  $\|\theta\|_1 < 1$  to ensure the causality of the time series when exogenous terms are bounded and known.

### 3.2 Estimation

The measurement error term in the proposed model, equation (3.2), improves the model robustness to model mis-specification and data errors, such as unobserved covariates for disease transmission and reporting errors in case data. However, it also brings difficulties in estimating  $R_t$  and parameters.

When  $\epsilon_t$  is assumed to be 0, equation (3.2) reduces to

$$h(R_t) = X_t^T \beta + \sum_{i=1}^q \theta_i f_i(D_{1,t}, D_{2,t}, D_{3,t}). \quad (3.4)$$

In this model, an estimator of the parameters  $\gamma = (\beta, \theta)$ , denoted as  $\hat{\gamma}$ , can be obtained by solving  $U_N(\gamma) = 0$ , where  $U_N(\gamma)$  is the quasi-score estimating function

$$U_N(\gamma) = \sum_{t=q}^N \left( \frac{\partial \mu_t}{\partial \gamma} \right)^T \nu_t^{-1} (I_t - \mu_t) \triangleq \sum_{t=q}^N \xi_t(\gamma). \quad (3.5)$$

Here, we assume the infectiousness function  $\omega = \{\omega_s, 1 \leq s \leq \eta\}$  is known in most practical scenarios, e.g., [He et al. \(2020\)](#) for COVID-19 viral shedding, assuming that some prior knowledge about the pathogen transmission profile has been reported previously. In situations when estimates of  $\omega$  are reported from multiple studies, we can conduct a meta-analysis to obtain a pooled estimate before plugging into equation (3.5). In cases when it is unknown, it can be estimated through (3.5) with a constraint  $\sum_{s=1}^{\eta} \omega_s = 1$  where  $\eta$  is known. In the rest of the manuscript, we assume  $\omega$  to be known unless otherwise stated.

When  $\epsilon_t$  is a non-degenerate random variable, calculating the expectation in  $\mu_t = \mathbb{E}[R_t|\mathcal{F}_{t-1}]\Lambda_t$  and solving  $U_N(\gamma) = 0$  are difficult in general. Similar models were studied by [Davis et al. \(2003\)](#) to model counts data using log link function, where the measurement error was assumed to be a stationary process and calculated using autoregressive moving average recursion with a distributed lag structure.

However, since we don't have direct observations ( $R_t$ ) for the time series (3.2) in this hierarchical model, so we describe an iterative method tailored for estimating parameters of (3.2), without requiring stationary structure and distribution assumption on the measurement error. Briefly, the proposed iterative algorithm consists of two steps. The first step uses the second layer of the model, the time series model, to construct a semi-parametric locally efficient estimator of  $\beta$  based on a location-shift regression model. In this step,  $\beta$  and  $R_t$  can be written as functions of  $\theta$  using an initial estimates of  $\theta$  or an estimate from the last iteration. In the second step, the parameters were updated using the first layer of the model, the quasi-score estimating function.

More specifically, we first rearrange the intercept term in  $X_t^T = (1, Z_t^T)$  into the autoregressive term. Then equation (3.2) can be rewritten as

$$h(R_t) - \sum_{i=1}^q \theta_i f_i(D_{1,t}, D_{2,t}, D_{3,t}) = Z_t^T \beta + \epsilon_t, \quad t = 1, \dots, N.$$

Assuming the Gauss-Markov assumption ([Wooldridge, 2016](#)), i.e, the conditional independence of  $\{\epsilon_t|X_t, t \geq 1\}$ ,  $\mathbb{E}[\epsilon_t|X_t] = 0$  and homoscedasticity, the above equation forms a location-shift regression model. Thus, given a  $\theta$  value, a semi-parametric locally efficient estimator ([Tsiatis, 2007](#)) for  $\beta$  is obtained by

$$\hat{\beta} = \left\{ \sum_{t=1}^N (Z_t - \bar{Z})(Z_t - \bar{Z})^T \right\}^{-1} \sum_{t=1}^N (Z_t - \bar{Z}) \left( h(R_t) - \sum_{i=1}^q \theta_i f_i(D_{1,t}, D_{2,t}, D_{3,t}) \right), \quad (3.6)$$

where  $\bar{Z} = (\sum_{t=1}^T Z_t)/N$  and  $N$  is the number of observations. Based on this formulation, we recommend an iterative method, namely the Quasi-score online estimation for infectious disease (QSOEID), to estimate  $\gamma$  and  $R_t$  by iteratively updating the locally-efficient semi-parametric estimator of  $\beta$  and the quasi-score estimator of  $\theta$  as shown in Algorithm 1. Intuitively, with an initial estimate of  $\theta$ , intermediate estimates of  $\beta$  and  $R_t$  can be written as functions of the initial estimate of  $\theta$  using equations (3.6) and (3.1) respectively. Then  $\theta$  can be further updated by solving equation (3.5). The algorithm is run iteratively until it converges.

Due to its iterative nature, this procedure provides an online estimator for  $\{R_t\}_{1 \leq t \leq N}$  and  $\gamma$  that can be updated daily or when data of new time points are available. The obtained estimates can also be used to forecast future  $\{R_t\}_{t > N}$  with projected covariates. Furthermore, these estimates and forecasts can be used to support policy-making by building a utility function to evaluate a set of interventions. For example, denote  $\hat{I}_{t+m}$  and  $\hat{R}_{t+m}$  as the forecasts from the proposed model, then for an intervention option  $A$  that belongs to the set of interventions  $\mathcal{S}$ , we may seek

$$\text{Optimal prevention option} = \min_{A \in \mathcal{S}} \mu(A)$$

$$\text{where } \mu(A) = \mu_1(\hat{I}_{t+m}) + \mu_2(\text{Economy}) + \mu_3(\text{Mental health}) + \mu_4(\text{Hospital capacity}) + \mu_5(\hat{R}_{t+m} \cdot \mathbb{1}(\hat{R}_{t+m} \geq 1) + \mathbb{1}(\hat{R}_{t+m} < 1)).$$

Here  $\mu_1 \sim \mu_5$  are utility functions for different social considerations. When  $\mu(A) \leq \mu(B) \Leftrightarrow A \preceq B$  it suggests  $A$  is preferred over  $B$ .

**Remark 3.1** *The procedure provides a forward-looking method to estimate  $R_t$ 's (Lipsitch et al., 2020), it can also be modified to provide backward-looking estimates as shown in section A of the supplementary material. In our simulation study, we found the back-looking*

---

**Algorithm 1** : The QSOEID algorithm

---

Estimation of the instantaneous reproduction number and covariates effects

---

- 1: **procedure** Initialize the parameters using data from a small initial period of the pandemic  $\tau_0$  and the model (3.4) that ignores measurement error. Denote the initial values as  $\hat{\theta}^{(\tau_0)}$ ,  $\hat{\beta}^{(\tau_0)}$  and  $\{\hat{R}_t^{(\tau_0)}\}_{0 < t \leq \tau_0}$ .
- 2:     **loop**
- 3:         **for**  $k > \tau_0$ , **and**  $k \leq N$ , **with** estimates  $\hat{\theta}^{(k-1)}$ ,  $\hat{\beta}^{(k-1)}$ , **and**  $\{\hat{R}_t^{(k-1)}\}_{0 < t \leq k-1}$  **obtained in last iteration, do**
- 4:             **write the approximations of  $\beta$  and  $\{R_t\}_{\tau_0+1 \leq t \leq k}$  as a function of  $\theta$  using equations (3.6) and (3.1), that is**

$$\begin{aligned} \tilde{\beta}^{(k)} &\triangleq \left\{ \sum_{t=1}^{k-1} (Z_t - \bar{Z}_{k-1})(Z_t - \bar{Z}_{k-1})^T \right\}^{-1} \\ &\quad \times \sum_{t=1}^{(k-1)} (Z_t - \bar{Z}_{k-1}) \left[ h(\hat{R}_t^{(k-1)}) - \sum_{s=1}^q \theta_s f_s(D_{1,t}, D_{2,t}, \hat{D}_{3,t}^{(k-1)}) \right] \end{aligned} \quad (3.7)$$

$$\text{and } \tilde{R}_t^{(k)} \triangleq h^{-1} \left( \sum_{s=1}^q \theta_s f_s(D_{1,t}, D_{2,t}, \hat{D}_{3,t}^{(k-1)}) + Z_t^T \tilde{\beta}^{(k)} \right), \quad (3.8)$$

- 5:         **Obtain  $\hat{\theta}^{(k)}$  by solving the quasi-score equation**

$$U_k(\theta) = \sum_{t=\tau_0+1}^k \left( \frac{\partial \tilde{\mu}_t^{(k)}}{\partial \theta} \right)^T (\tilde{\nu}_t^{(k)})^{-1} (I_t - \tilde{\mu}_t^{(k)}) \quad (3.9)$$

using iterative methods, e.g. Newton-Raphson and iteratively reweighted least squares, where  $\tilde{\mu}_t^{(k)} = \tilde{\nu}_t^{(k)} \triangleq \tilde{R}_t^{(k)} \Lambda_j$ .

- 6:         **Obtain  $\hat{\beta}^{(k)}$  and  $\{\hat{R}_t^{(k)}\}_{1 \leq t \leq k}$  by plugging  $\hat{\theta}^{(k)}$  into (3.7) and (3.8) as follows**

$$\begin{aligned} \hat{\beta}^{(k)} &\triangleq \left\{ \sum_{t=1}^{k-1} (Z_t - \bar{Z}_{k-1})(Z_t - \bar{Z}_{k-1})^T \right\}^{-1} \\ &\quad \times \sum_{t=1}^{k-1} (Z_t - \bar{Z}_{k-1}) \left[ h(\hat{R}_t^{(k-1)}) - \sum_{s=1}^q \hat{\theta}_s^{(k)} f_s(D_{1,t}, D_{2,t}, \hat{D}_{3,t}^{(k-1)}) \right], \end{aligned} \quad (3.10)$$

$$\text{and } \hat{R}_t^{(k)} \triangleq h^{-1} \left( \sum_{s=1}^q \hat{\theta}_s^{(k)} f_s(D_{1,t}, D_{2,t}, \hat{D}_{3,t}^{(k)}) + Z_t^T \hat{\beta}^{(k)} \right). \quad (3.11)$$

- 7:         **end for**

- 8:         **end loop**

- 9: **end procedure**

---

estimator (supplementary materials A.1) performs similarly with much less computing time and less sensitivity to initial values. In practice, whether to use the forward-looking or the forward-looking method is a trade-off between accuracy and computational cost.

### 3.3 Uncertainty quantification

The block bootstrap method introduced by Hall (1985) and Künsch (1989) can be used to quantify the uncertainty of the proposed online estimator. Here we illustrate the calculation for  $\beta$ . Given the time series case counts and covariates,  $\{(I_t, Z_t)\}_{1 \leq t \leq N}$ , where  $Z_t$  is a  $p$ -dimensional vector of covariates at time  $t$ , we assume  $\beta$  is estimable using a block of data as long as the length of the block exceeds  $\ell$ , i.e., we require  $(\sum_{t \in \mathcal{S}} (Z_t - \bar{Z}_{\mathcal{S}})(Z_t - \bar{Z}_{\mathcal{S}})^T)^{-1}$  to be well defined for arbitrary set  $\mathcal{S} \subset \{1, \dots, N\}$  with  $|\mathcal{S}| \geq \ell$ .

Denote a block of data up to time  $t$  with length  $\ell$  as  $\xi_t = \left( (I_{t-\ell+1}, Z_{t-\ell+1}), \dots, (I_t, Z_t) \right)$  for  $t = \ell, \dots, N$ . We adopt the suggested  $\ell = O(N^{1/3})$  from Bühlmann and Künsch (1999) and independently resample  $s$  blocks of data with replacement, for  $s = O(\lfloor (N - p - \tau_0)/\ell \rfloor)$  (Bühlmann, 2002) to obtain  $s$  bootstrap samples  $\xi_{t_1}, \xi_{t_2}, \dots, \xi_{t_s}$ . For the effect of  $j$ -th covariate,  $\beta_j$ , where  $j = 1, \dots, p$ , denote the estimator based on the  $i$ -th sample as  $\hat{\beta}_{t_i,j}^*$  and the estimator using the whole data as  $\hat{\beta}_j$ . One may use  $\{\hat{\beta}_{t_i,j}^* - \hat{\beta}_j : i = 1, \dots, s\}$  to approximate the empirical distribution of  $(\hat{\beta}_j - \beta_j)$  or use  $\{\hat{\beta}_{t_i,j}^* : i = 1, \dots, s\}$  as an approximation of the empirical distribution of  $\hat{\beta}_j$ . Thus the level  $1 - \alpha$  bootstrap confidence interval of  $\beta_j$  based on the  $s$  samples,  $(L_{j,\alpha/2,s}^*, U_{j,\alpha/2,s}^*)$ , can be constructed by

$$\begin{aligned} L_{j,\alpha/2,s}^* &= 2\hat{\beta}_j - \sup \left\{ t : \frac{1}{s} \sum_{i=1}^s \mathbb{1}(\hat{\beta}_{t_i,j}^* \leq t) \leq 1 - \frac{\alpha}{2} \right\}, \\ U_{j,\alpha/2,s}^* &= 2\hat{\beta}_j - \inf \left\{ t : \frac{1}{s} \sum_{i=1}^s \mathbb{1}(\hat{\beta}_{t_i,j}^* \leq t) \geq \frac{\alpha}{2} \right\}, \quad \text{or} \end{aligned} \quad (3.12)$$

$$L_{j,\alpha/2,s}^* = \inf \left\{ t : \frac{1}{s} \sum_{i=1}^s \mathbb{1}(\hat{\beta}_{t_i,j}^* \leq t) \geq \frac{\alpha}{2} \right\}, \quad U_{j,\alpha/2,s}^* = \sup \left\{ t : \frac{1}{s} \sum_{i=1}^s \mathbb{1}(\hat{\beta}_{t_i,j}^* \leq t) \leq 1 - \frac{\alpha}{2} \right\}.$$

The confidence band of  $\{\hat{R}_t\}_{t \geq 0}$  can be obtained similarly using the empirical quantiles of  $\{\hat{R}_{t_i,t}^*, 1 \leq i \leq s\}_{t \geq 0}$  calculated from the bootstrap estimators of model parameters.

## 4 Properties of the Estimator and Algorithm

### 4.1 Asymptotic properties

The proposed method is a general approach for different counting processes and is robust to mis-specification of distribution assumptions. When the measurement error is ignored, i.e.  $\epsilon_t = 0$ , the Poisson process used in (Cori et al., 2013) is a special case of (3.1) with  $\nu_t = \mu_t$ . Since  $U_t(\gamma) \in \mathcal{F}_t$  and  $\partial\mu_t/\partial\gamma, \mu_t, \nu_t \in \mathcal{F}_{t-1}$ , then  $\{(U_s(\gamma), \mathcal{F}_s), s \geq q\}$  is a mean zero martingale sequence, indicating that  $U_N(\gamma)$  is an unbiased estimating function. Denote the oracle parameter value as  $\gamma_0$  and according to theorem 3 of Kaufmann (1987), we have

**Theorem 4.1** *Under condition 1 described in section B of the supplementary material and on the non-extinction set defined in (B.1),*

$$\left[ \sum_{t=q}^N \text{Cov}(\xi_t(\gamma_0) | \mathcal{F}_{t-1}) \right]^{1/2} (\hat{\gamma} - \gamma_0) \xrightarrow{d} \mathcal{N}(0, I). \quad (4.1)$$

In supplementary material section B, we also show a special case of (3.4), given by

$$\log(R_t) = x_t^T \beta + \sum_{i=1}^q \theta_i [\log(R_{t-i}) - x_{t-i}^T \beta], \quad \text{for } t \geq q > 0, \quad \theta_i \geq 0, \quad \text{and } \|\theta\|_1 < 1, \quad (4.2)$$

satisfies (4.1) under a more traceable condition 2.

## 4.2 Bias correction and property of the estimation procedure

When the measurement error cannot be ignored, the proposed iterative algorithm consists of two major steps: one utilizes the semi-parametric locally efficient estimator to write  $\beta$  and  $R_t$  as a function of  $\theta$  and the other updates the estimates by solving the score equation. However, the latter step is subject to estimation bias due to the bias of the score equation with the non-zero measurement error term from equation (3.2) (Cameron and Trivedi, 2013). Bias correction in the general case (3.2) is difficult, but it can be tackled in (3.3) by requiring  $\mathbb{E}(e^{\epsilon_t}|\mathcal{F}_{t-1}) = c_0$  for some constant  $c_0$  (Zeger, 1988). Therefore, we can correct the bias by modifying the quasi-score equation (3.9) to an unbiased estimating equation as follows

$$U_k^*(\phi_0, \theta) = \sum_{t=\tau_0+1}^k \left( \frac{\partial \tilde{\mu}_t^{(k)}}{\partial \theta} \right)^T \left( \tilde{\nu}_t^{(k)} \right)^{-1} (I_t/c_0 - \tilde{\mu}_t^{(k)}).$$

In practice,  $c_0$  can be treated as a nuisance parameter and estimated by solving the quasi-score equation. Moreover, under (3.3), solving the modified quasi-score equation (3.9) is equivalent to obtaining

$$(\hat{\phi}_0^{(k)}, \hat{\theta}^{(k)}) = \arg \max_{\|\theta\|_1 < 1} \sum_{t=\tau_0+1}^k \left( I_t \log \tilde{R}_t^{(k)} - \tilde{R}_t^{(k)} \Lambda_t \right), \quad (4.3)$$

where  $(\hat{\phi}_0^{(k)}, \hat{\theta}^{(k)})$  is the MLE based on conditional profile likelihood of Poisson counts. Therefore, the proposed online estimation procedure guarantees the following properties. Proof of the theorems is presented in section *C* of the supplementary material.

**Theorem 4.2 (Concavity)** *When  $k > \tau_0$ , to update estimates in each iteration, equivalently to solve equation (4.3), is a globally concave maximization problem.*

**Theorem 4.3 (Iteration Difference)** *Given regularity condition 3 in the supplementary material and observed case counts and covariates up to time  $N$ ,  $\{(I_t, Z_t)\}_{1 \leq t \leq N}$ , for each  $1 \leq i \leq q$ ,*

$$|\hat{\theta}_i^{(k)} - \hat{\theta}_i^{(k-1)}| = O\left(\frac{1}{k-1} + \frac{I_k}{(\sum_{t=\tau_0+1}^{k-1} I_n)}\right),$$

where  $k \leq N$  is the indicator of iteration.

Theorem 4.3 demonstrates the bound of step-wise difference of the online estimator between iterations, which decreases as the number of observation time increases. The above form was obtained using the backward-looking algorithm. Results of the forward-looking algorithm, which shares a similar form, is shown in supplementary material. But, the estimator's consistency remains an open question as discussed in [Davis et al. \(2003\)](#). The difficulty arise from the measurement error  $\{\epsilon_s\}_{s \geq 1}$  and the disease case series dependency  $\{\Lambda_{s \geq 1}\}$  in the model. However, both elements are essential in modeling the dynamics of disease transmission. The measurement error is a major issue in the disease counts and covariates data, and  $\{\Lambda_{s \geq 1}\}$  is the key feature describing the dynamic of infection. Similar but simplified models, which do not model the measurement errors and  $\{\Lambda_{s \geq 1}\}$  are built for different contexts, e.g. studies of economics or disease without case series dependency ([Davis et al., 1999, 2000, 2003; Fokianos et al., 2009; Neumann et al., 2011; Doukhan, Fokianos and Li, 2012; Doukhan, Fokianos and Tjøstheim, 2012](#)). Inspired by the derivation and discussion in [Davis et al. \(2003\)](#), we conjecture that conditions requiring stationary and uniformly ergodic of  $\log(R_t \Lambda_t)$  are needed to establish the consistency of estimators of model (3.3), although these conditions may be difficult to verify in practice.

## 5 Simulation Studies

This section describes the simulation studies we conducted to assess the performance of the proposed method, including the relative bias, coefficient of variation of the estimates, and the coverage probability of the Bootstrap confidence interval, with a focus on the estimation of covariates effect size that motivates the study. In addition, a comparison between the proposed model and basic SIR model is presented in the supplementary material.

### 5.1 Simulation settings

Throughout the simulation, we generated daily data of SARS-CoV-2 case counts and associated covariates, and fit the semi-parametric time series model (3.3) which assumed the  $R_t$ 's have AR(1) dependency and were associated with two covariates, i.e.,  $q = 1$  and  $p = 2$ . Each scenario was repeated for 1,000 times to calculate the evaluation statistics. The infectivity function was assumed to be known and generated from a gamma distribution to mimic the result in a previous epidemiological study of SARS-CoV-2 cases in Wuhan, China (Li et al., 2020).

Data were simulated under various scenarios, including settings for which the fitted models were correctly specified or mis-specified. For scenarios with correctly specified models (scenarios 1-7), data were generated using parameters  $(\phi_0, \theta_1, \beta_1, \beta_2) = (.5, .7, -.02, -.125)$ , where the simulated  $\{R_t, t \geq 1\}$  mimicked the trend of the  $R_t$  reported in Pan, Liu, Wang, Guo, Hao, Wang, Huang, He, Yu, Lin et al. (2020). We varied days of observation  $T$ , initial incident cases  $I_0$ , and used different distributions of error terms  $\{\epsilon_t \sim_{i.i.d} \epsilon, t = 1, \dots, T\}$  to generate data. For settings in which the model was mis-specified (scenarios 8-9), data were simulated assuming  $R_t$ 's followed AR(2) dependency (i.e.,  $q = 2$ ) or three covari-

ates (i.e.,  $p = 3$ ). The two daily covariates were simulated independently to mimic the real data of temperature in Philadelphia and data of social distancing from daily cellular telephone movement, provided by Unacast ([Unacast, 2021, July 1st](#)), which measured the percent change in visits to nonessential businesses, e.g., restaurants and hair salons during March 1st and June 30th, 2020. Details of parameter values used in each scenario and the generating distribution of covariates data are shown in Section [A.2](#) of the supplementary materials.

Table 1: Relative bias, bias and coefficient of variation of the estimators, calculated by  $\sum_{i=1}^{N_s} (\hat{\theta}_i - \theta) / N_s \theta$ ,  $\sum_{i=1}^{N_s} (\hat{\theta}_i - \theta) / N_s$  and  $\{\sum_{i=1}^{N_s} [\hat{\theta}_i - (\sum_{i=1}^{N_s} \hat{\theta}_i / N_s)]^2\}^{1/2} / (\sum_{i=1}^{N_s} \hat{\theta}_i / N_s)$  with  $N_s = 1000$  replicates.  $\hat{\theta}$  indicates the estimated value and  $\theta$  is the true value.

<b>Scenario</b>	relative bias (%)				empirical bias ( $\times 10^{-2}$ )				coefficient of variation $\hat{\sigma}/\hat{\mu}$			
	$\phi_0$	$\theta_1$	$\beta_1$	$\beta_2$	$\phi_0$	$\theta_1$	$\beta_1$	$\beta_2$	$\phi_0$	$\theta_1$	$\beta_1$	$\beta_2$
<b>1</b>	-2.41	-1.42	-0.34	5.03	-1.20	-0.99	-0.01	0.63	0.27	0.11	0.36	0.36
<b>2</b>	-2.94	-1.51	-1.19	6.26	-1.47	-1.05	-0.02	0.78	0.37	0.10	0.55	0.38
<b>3</b>	-1.15	-0.78	-0.47	2.19	-0.57	-0.55	-0.01	0.27	0.24	0.10	0.27	0.29
<b>4</b>	-2.08	-3.57	-0.04	7.18	-1.04	-2.50	-0.00	0.90	0.37	0.14	0.69	0.64
<b>5</b>	-4.87	-1.85	-5.67	5.00	-2.44	-1.29	-0.11	0.63	0.39	0.13	0.98	0.60
<b>6</b>	-1.10	-4.16	-4.47	6.90	-0.55	-2.91	-0.09	0.86	0.39	0.13	0.43	0.48
<b>7</b>	-4.20	-1.43	-0.53	8.22	-2.10	-1.00	-0.01	1.03	0.28	0.11	0.37	0.36
<b>8</b>	-17.83	-0.72	4.06	9.64	-8.92	-0.51	0.14	1.20	0.31	0.12	0.31	0.42
<b>9</b>	/	/	-17.67	9.95	/	/	-3.53	1.24	/	/	0.27	0.27

## 5.2 Simulation results

Table 1 shows the bias and coefficient of variation of the estimators in each scenario. In scenarios 1 – 5, both the bias and the coefficient of variation decreased as the sample size or initial case count  $I_0$  increased. The proposed estimator still showed good performance with a relatively larger bias and variance when the error term's variance was increased up to a magnitude that was smaller than the product of covariates and their corresponding effect sizes (scenarios 1 vs 6). When the error term had a heavier tail (scenario 7), the algorithm still had robust performance.

Two types of mis-specification (scenarios 8 and 9) were considered. In scenario 8, an important time-varying covariate was omitted from the model. Due to the correlation between generated covariates through time, this scenario is different from increasing the error term's variance only. In both mis-specified cases, estimators  $(\hat{\phi}_0, \hat{\theta})$  were close to the corresponding partial correlation coefficient rather than the oracle value. Although the mis-specification caused an increasing in estimation bias but the algorithm still provides a relatively accurate estimator for correctly specified parts, with small bias and coefficient of variation (scenarios 1, 8 and 9). Most importantly, as illustrated in Figure 3 from a random replication of the simulation, the estimated  $R_t$ 's still captured the tendency of oracle  $\{R_t\}_{t \geq 0}$  especially when the time-series' sample size increases.

We also constructed the bootstrap confidence interval according to (3.12) and the coverage probability of bootstrap confidence interval for  $\beta_1$  is shown in Table 2 as an illustration. Table 2 confirms that the proposed bootstrap confidence interval provides the expected coverage probability when chosen  $\ell = 45 = \tau_0 + O(T^{1/3})$  for  $T = 300$  following the recommendations in Bühlmann and Künsch (1999) and set the number of replications  $k = 500 = O(T^{2/3})$  following Bühlmann (2002). When a smaller block length  $\ell = 30$  is

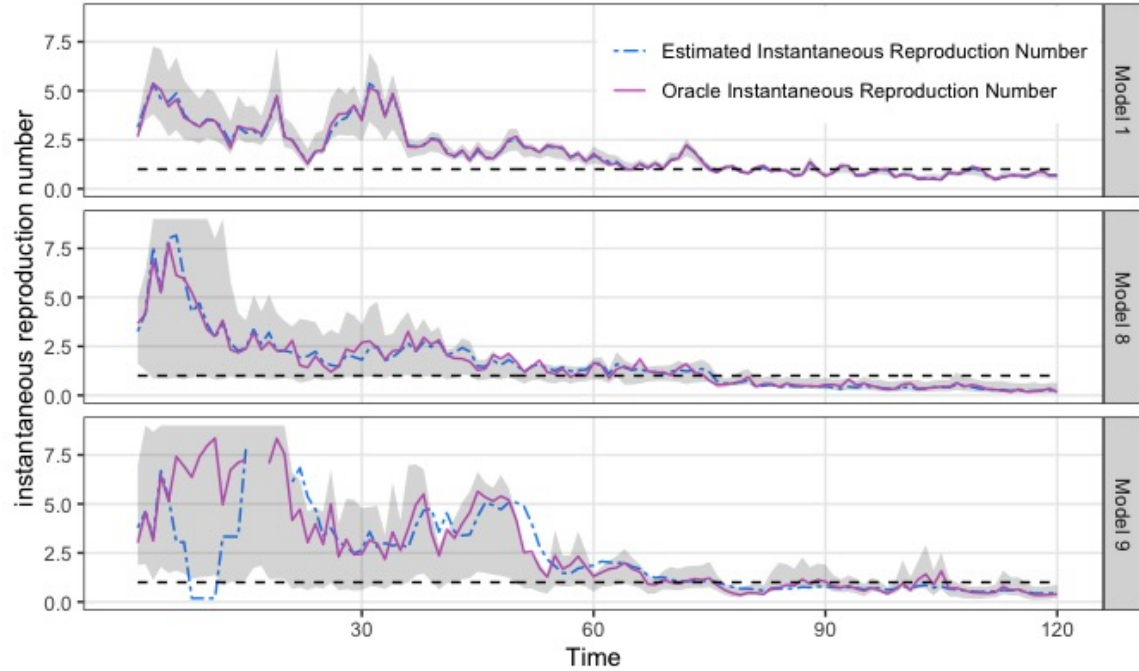


Figure 3: Estimated  $R_t$ 's and 90% bootstrap confidence bands from random replications of simulation, with block length  $\ell = 45$  and bootstrap replication  $k = 200$ .

Table 2: Coverage Probability of  $1 - \alpha$  Empirical Bootstrap Confidence Interval for  $\phi_0$

	T=300 $\ell = 30$	T=300 $\ell = 45$	T=300 $\ell = 60$	T=450 $\ell = 30$	T=450 $\ell = 45$
$\alpha = 5\%$	96.4%	94.8%	93.0%	99.8%	99.2%
$\alpha = 10\%$	91.2%	87.8%	86.2%	98.6%	97.2%
$\alpha = 20\%$	83.4%	79.8%	77.2%	96.8%	93.2%

chosen for  $T = 300$ , the accuracy of the Bootstrap estimator is decreased compared to  $\hat{\beta}_1$ , leading to a conservative confidence interval. On the contrast, when a larger block length  $\ell = 60$  is chosen, despite the bootstrap estimator has better accuracy, the coverage probability is less than ideal due to high correlation between bootstrap subsample. Besides, the optimal block length also relates to  $T$ , as  $\ell = 30$  and  $\ell = 45$  would only results in a conservative confidence interval. Practically, we suggest to choose the smaller  $\ell$  that satisfies  $\ell = O(N^{1/3})$  from [Bühlmann and Künsch \(1999\)](#).

## 6 Application to COVID-19 Data

We applied the proposed method to a dataset which contained daily COVID-19 case count from 517 US counties representing 46 states and the District of Columbia between February 1st and July 6th 2020 and county level covariates, including demographics, social distancing measures and temperature variables. To be eligible, a county had to have  $\varrho$  incident cases for more than two out of six consecutive days for at least 20 times (e.g.,  $\varrho = 5$ ), as of June 1st, 2020 and meet at least one of the following criteria: 1) contained at least one city with population exceeding 100,000 persons; 2) contained a state capital; 3) the county was the most populated county in the state; or 4) average daily case incidence exceeded 20 during June 1st to June 30th, 2020. Within county, accumulative case count before the first  $\varrho$  incidence cases was considered as  $I_0$ . As a sensitivity analysis, we explored three different  $\varrho$  values, i.e.  $\varrho = 10, 15$ , and the analyses showed similar results so we presented the results with  $\varrho = 10$ . The incidence threshold of 20 in 4) was selected based on empirical distribution of case counts in the observation time period. Daily incidence case count were smoothed using a 4-day moving average to reduce the impact of batch reporting. Our goals

were to examine the association between county-level factors and  $R_t$ , to forecast the future case count, and to provide evidence for selecting appropriate social distancing policies.

## 6.1 Covariates selection and data preparation

We inherit three covariates described in an early study by [Rubin et al. \(2020\)](#): population density, social distancing and wet-bulb temperature. Social distancing is measured by a percent change in visits to nonessential businesses (e.g., restaurants, hair salons) revealed by daily cell-phone movement within each county, compared with visits in a four-week baseline period between February 10th and March 8th, 2020. Wet-bulb temperature is invoked since it has been demonstrated that humidity and temperature both play role in the seasonality of influenza. Further, a moving average with window length 11 days and a lag operator with delay of 3 days are imposed on the social distancing covariates and wet-bulb temperatures, based on the lag observed between change in social distancing and  $R_t$  estimates and on an incubation period of at least 3 days. Other county-level covariates that we also considered includes demographic factors (e.g., age distribution, insurance status, etc), health-related factors (e.g., obesity, diabetes and proportion of individuals who smoke.), policy-related factors (e.g., mask wearing restrictions). Based on the correlation among the variables, we chose elderly population percentage from sociology related covariates and chose population percentage of diabetes from medical related covariates in the final model.

## 6.2 Covariates effect size estimation and interpretation

The estimates and corresponding bootstrap intervals were demonstrated in Table 3. We found that, in addition to the strongest factor social distancing, population density, the percentage of elderly population and the percentage of diabetic population were also posi-

Table 3: Parameter estimates and bootstrap intervals from analyzing the county level COVID-19 data from 517 US counties between February 1st and July 6th 2020.

$\alpha$	$\varrho^1$	Elderly Pop. %,		Pop. Density	Diabetes %	Social Dist.	Wet-bulb Temp.
		$\beta_1$	$\beta_2 (\times 10^{-2})$				
0.05	10	2.438 (0.833, 5.633)	2.001 (-0.771, 5.373)	6.666 (1.848, 9.734)	0.608 (0.298, 1.624)	0.608 (-2.519, -0.485)	-2.209
	15	2.660 (1.335, 5.624)	3.695 (1.639, 7.541)	7.159 (2.004, 11.43)	0.726 (0.576, 1.848)	0.726 (-2.625, -0.443)	-2.273
	10	(0.970, 5.154)	(-0.522, 4.944)	(2.006, 9.624)	(0.328, 1.404)	(0.328, 1.404)	(-2.343, -0.539)
	15	(1.403, 5.542)	(1.745, 6.484)	(2.127, 11.19)	(0.633, 1.672)	(0.633, 1.672)	(-2.537, -0.494)

<sup>1</sup>. For  $\varrho = 10$  and 15, there are 444 and 364 counties and 38828 and 30177 observations, respectively. Bootstrap replication  $k = 200$  and block length  $\ell = 45$ . Additional results from different  $\varrho$  and  $\ell$  values can be found in supplementary materials A.3.

tively associated with  $R_t$ . It suggested that densely populated metropolitan counties with higher percentage of senior and diabetic population could have worse outbreaks comparing to rural counties with younger and healthier population. Note that temperature had negative impact on  $R_t$ , suggesting the transmission could slow down in warm weather. Although the effect size of temperature,  $\hat{\beta}_5$ , was small, its impact on policy making may be substantial, due to the wide range of temperature a county could experience within a year. During the study period, the largest increment of wet-bulb temperatures observed within a county was  $32.8^\circ\text{C}$ , which could reduce the transmission of COVID-19 by 51.5% with other covariates fixed. However, temperature could also affect social distancing values, as outdoor activities tended to increase during spring and summer, which could cancel out the reduction of transmission from increased temperature.

### 6.3 Estimating $R_t$ and forecasting future transmission

County-level  $R_t$ 's were estimated using the proposed QSOEID algorithm and backward estimation. The results clearly illustrated the evolution of the pandemic and the change of outbreak epicenter during the study period (Figure 4A). Due to space limit, we left more details on results interpretation and discussion to A.4 of supplementary materials. Based on the parameter estimates and projected values of covariates, we can forecast county-level disease transmission by calculating future  $R_t$  and case count using the proposed model. In this application, we set social distancing value at three values,  $-61.25\%$ ,  $-35\%$  and  $0\%$ , to mimic the social distancing level under the reopening orders at Phase 1, Phase 3 and Phase 5 (without restriction), and used historical 10-year-average wet-bulb temperature to project the disease transmission. The three levels of social distancing were estimated by averaging data between May and June under different reopening orders. Taking the prediction at September 1st as an example, which is 57 days after the last day of the dataset. The predicted  $R_t$  in Figure 4B presented the difference under different restrictions. These results can be used to support selection of intervention.

## 7 Discussion

In this paper, we proposed a novel model to predict and monitor disease transmission, evaluate covariates impact and investigate the generative nature of the virus. The time series dependency among the incidence case counts were decomposed into an epidemiological part, which was modeled using the TSI model, and a statistical part, which was modeled using an observed-driven model. We used the quasi-score method, together with an online algorithm, to estimate the instantaneous reproduction number and effects of covariates

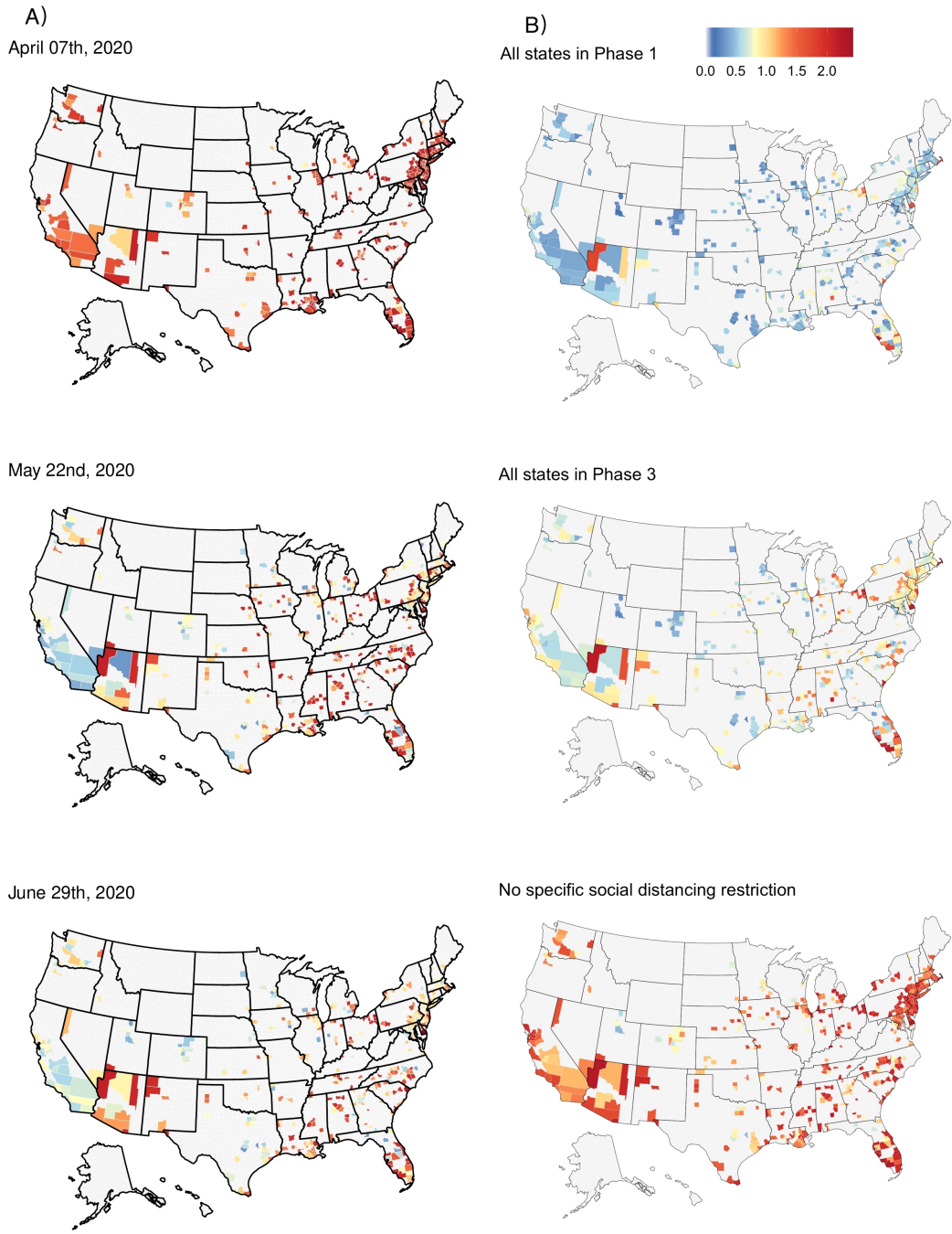


Figure 4: Heat maps for estimated and predicted county-level  $R_t$  across United States. Roughly,  $0 < R_t < 0.9$  : bluish,  $0.9 \leq R_t \leq 1.1$  : yellowish,  $R_t > 1.1$  : Reddish. Column A) shows estimated  $R_t$  at three time points, which illustrates the shift of epicenter during April to June 2020. Column B) demonstrates predicted  $R_t$  on September 1st based on three levels of social distancing

on disease transmission simultaneously. Our method contributed an exquisite gadget to a much larger toolbox in fighting the coronavirus pandemic.

Yet there are many feasible extensions of the model that are worth mentioning. Here we provide several hoping to inspire future discussion on possible improvements. First, the proposed method can be extended to a nonparametric model by relaxing the assumption on link function to avoid mis-specification (supplementary materials A.5). The estimation is straightforward if the dependency of  $\{R_t\}_{t \geq 0}$  is ignored. When time series dependency of  $\{R_t\}_{t \geq 0}$  is considered, e.g.,  $\mathbb{E}[R_t | Z_t, D_{3,t}] = \phi_0 + \sum_{i=1}^q \theta_i f_i(R_{t-i}) + g(Z_t)$  with a known  $R_0$  and known functions  $f_i$ ,  $1 \leq i \leq q$  and unknown  $g(\cdot)$ , we can adopt local linear kernel estimators (Fan and Gijbels, 1996) into the proposed iterative algorithm. Second, the proposed method can be extended to model data from multiple regions using a random effect model (supplementary materials A.6) with an adapted distributional assumption on the random effect for individual region.

The proposed method also has a few limitations. First, heterogeneous testing capacity across the country and over time is a big challenge to the data quality. The errors due to testing capacity can be partially absorbed into the measurement error term in the proposed method, but without knowing the distribution of testing capacity (very likely changing over time), the proposed extension in supplementary materials A.6 may still fail to correct the bias rooted from these data errors. Another possible method to address this limitation is to use seroprevalence surveillance data to estimate the testing capacity, which will require the availability of additional data (Quick et al., 2021). Another limitation of the proposed method is related to the limitation of the TSI model, which uses only the incidence case data to estimate the instantaneous reproduction number. This leads to the fact that the performance of the proposed method could rely on the quality of case data. Although we

proposed to use a measurement error term to address this challenge, it would be worthwhile to develop TSI models that can incorporate death or hospital admission data in future research.

## References

Ardabili, S. F., Mosavi, A., Ghamisi, P., Ferdinand, F., Varkonyi-Koczy, A. R., Reuter, U., Rabczuk, T. and Atkinson, P. M. (2020), ‘Covid-19 outbreak prediction with machine learning’, *Algorithms* **13**(10), 249.

Boatto, S., Bonnet, C., Cazelles, B. and Mazenc, F. (2018), ‘Sir model with time dependent infectivity parameter: approximating the epidemic attractor and the importance of the initial phase.’.

Bühlmann, P. (2002), ‘Bootstraps for time series’, *Statistical science* pp. 52–72.

Bühlmann, P. and Künsch, H. R. (1999), ‘Block length selection in the bootstrap for time series’, *Computational Statistics & Data Analysis* **31**(3), 295–310.

Cameron, A. C. and Trivedi, P. K. (2013), *Regression analysis of count data*, Vol. 53, Cambridge university press.

Cevik, M., Tate, M., Lloyd, O., Maraolo, A. E., Schafers, J. and Ho, A. (2021), ‘Sars-cov-2, sars-cov, and mers-cov viral load dynamics, duration of viral shedding, and infectiousness: a systematic review and meta-analysis’, *The lancet microbe* **2**(1), e13–e22.

Chen, Y.-C., Lu, P.-E. and Chang, C.-S. (2020), ‘A time-dependent sir model for covid-19’, *arXiv preprint arXiv:2003.00122* .

Cori, A., Ferguson, N. M., Fraser, C. and Cauchemez, S. (2013), ‘A new framework and software to estimate time-varying reproduction numbers during epidemics’, *American journal of epidemiology* **178**(9), 1505–1512.

Costa-Santos, C., Neves, A. L., Correia, R., Santos, P., Monteiro-Soares, M., Freitas, A., Ribeiro-Vaz, I., Henriques, T. S., Rodrigues, P. P., Costa-Pereira, A. et al. (2021), ‘Covid-19 surveillance data quality issues: a national consecutive case series’, *BMJ open* **11**(12), e047623.

Davis, R. A., Dunsmuir, W. T. and Streett, S. B. (2003), ‘Observation-driven models for poisson counts’, *Biometrika* **90**(4), 777–790.

Davis, R. A., Dunsmuir, W. T. and Wang, Y. (1999), ‘Modeling time series of count data’, *Statistics Textbooks and Monographs* **158**, 63–114.

Davis, R. A., Dunsmuir, W. T. and Wang, Y. (2000), ‘On autocorrelation in a poisson regression model’, *Biometrika* **87**(3), 491–505.

Dayan, I., Roth, H. R., Zhong, A., Harouni, A., Gentili, A., Abidin, A. Z., Liu, A., Costa, A. B., Wood, B. J., Tsai, C.-S. et al. (2021), ‘Federated learning for predicting clinical outcomes in patients with covid-19’, *Nature medicine* pp. 1–9.

Doukhan, P., Fokianos, K. and Li, X. (2012), ‘On weak dependence conditions: the case of discrete valued processes’, *Statistics & Probability Letters* **82**(11), 1941–1948.

Doukhan, P., Fokianos, K. and Tjøstheim, D. (2012), ‘On weak dependence conditions for poisson autoregressions’, *Statistics & Probability Letters* **82**(5), 942–948.

Fan, J. and Gijbels, I. (1996), *Local polynomial modelling and its applications: monographs on statistics and applied probability 66*, Vol. 66, CRC Press.

Fokianos, K., Rahbek, A. and Tjøstheim, D. (2009), ‘Poisson autoregression’, *Journal of the American Statistical Association* **104**(488), 1430–1439.

Fraser, C. (2007), ‘Estimating individual and household reproduction numbers in an emerging epidemic’, *PloS one* **2**(8), e758.

Hall, P. (1985), ‘Resampling a coverage pattern’, *Stochastic processes and their applications* **20**(2), 231–246.

He, X., Lau, E. H., Wu, P., Deng, X., Wang, J., Hao, X., Lau, Y. C., Wong, J. Y., Guan, Y., Tan, X. et al. (2020), ‘Temporal dynamics in viral shedding and transmissibility of covid-19’, *Nature medicine* **26**(5), 672–675.

IHME COVID-19 forecasting team (2020), ‘Modeling covid-19 scenarios for the united states’, *Nature medicine* .

Kaufmann, H. (1987), ‘Regression models for nonstationary categorical time series: asymptotic estimation theory’, *The Annals of Statistics* pp. 79–98.

Kermack, W. O. and McKendrick, A. G. (1927), ‘A contribution to the mathematical theory of epidemics’, *Proceedings of the royal society of london. Series A, Containing papers of a mathematical and physical character* **115**(772), 700–721.

Künsch, H. R. (1989), ‘The jackknife and the bootstrap for general stationary observations’, *Annals of Statistics* **17**(3), 1217–1241.

Li, Q., Guan, X., Wu, P., Wang, X., Zhou, L., Tong, Y., Ren, R., Leung, K. S., Lau, E. H., Wong, J. Y. et al. (2020), ‘Early transmission dynamics in wuhan, china, of novel coronavirus–infected pneumonia’, *New England journal of medicine* .

Lipsitch, M., Joshi, K. and Cobey, S. E. (2020), ‘Comment on pan a, liu l, wang c, et al.,’ association of public health interventions with the epidemiology of the covid-19 outbreak in wuhan, china,’ *jama*, published online april 10, 2020’.

Neumann, M. H. et al. (2011), ‘Absolute regularity and ergodicity of poisson count processes’, *Bernoulli* **17**(4), 1268–1284.

Pan, A., Liu, L., Wang, C., Guo, H., Hao, X., Wang, Q., Huang, J., He, N., Yu, H., Lin, X. et al. (2020), ‘Association of public health interventions with the epidemiology of the covid-19 outbreak in wuhan, china’, *Jama* **323**(19), 1915–1923.

Pan, T., Shen, W. and Hu, G. (2020), ‘Spatial homogeneity learning for spatially correlated functional data with application to covid-19 growth rate curves’, *arXiv preprint arXiv:2008.09227* .

Punn, N. S., Sonbhadra, S. K. and Agarwal, S. (2020), ‘Covid-19 epidemic analysis using machine learning and deep learning algorithms’, *MedRxiv* .

Quick, C., Dey, R. and Lin, X. (2021), ‘Regression models for understanding covid-19 epidemic dynamics with incomplete data’, *Journal of the American Statistical Association* **116**(536), 1561–1577.

Rubin, D., Huang, J., Fisher, B. T., Gasparrini, A., Tam, V., Song, L., Wang, X., Kaufman, J., Fitzpatrick, K., Jain, A. et al. (2020), ‘Association of social distancing, population

density, and temperature with the instantaneous reproduction number of sars-cov-2 in counties across the united states', *JAMA network open* **3**(7), e2016099–e2016099.

Sáez, C., Romero, N., Conejero, J. A. and García-Gómez, J. M. (2021), 'Potential limitations in covid-19 machine learning due to data source variability: A case study in the ncov2019 dataset', *Journal of the American Medical Informatics Association* **28**(2), 360–364.

Song, P. X., Wang, L., Zhou, Y., He, J., Zhu, B., Wang, F., Tang, L. and Eisenberg, M. (2020), 'An epidemiological forecast model and software assessing interventions on covid-19 epidemic in china', *MedRxiv* .

Tian, T., Tan, J., Jiang, Y., Wang, X. and Zhang, H. (2020), 'Evaluate the risk of resumption of business for the states of new york, new jersey and connecticut via a pre-symptomatic and asymptomatic transmission model of covid-19', *Journal of Data Science* p. 1.

Tsiatis, A. (2007), *Semiparametric theory and missing data*, Springer Science & Business Media.

Unacast (2021, July 1st), 'Social distancing scoreboard'.

**URL:** <https://www.unacast.com/covid19/socialdistancing-scoreboard#methodology>

Wallinga, J. and Teunis, P. (2004), 'Different epidemic curves for severe acute respiratory syndrome reveal similar impacts of control measures', *American Journal of epidemiology* **160**(6), 509–516.

Wang, L., Zhou, Y., He, J., Zhu, B., Wang, F., Tang, L., Kleinsasser, M., Barker, D.,

Eisenberg, M. C. and Song, P. X. (2020), ‘An epidemiological forecast model and software assessing interventions on the covid-19 epidemic in china’, *Journal of Data Science* **18**(3), 409–432.

WHO Ebola Response Team (2014), ‘Ebola virus disease in west africa—the first 9 months of the epidemic and forward projections’, *New England Journal of Medicine* **371**(16), 1481–1495.

Wooldridge, J. M. (2016), *Introductory econometrics: A modern approach*, Nelson Education.

Zeger, S. L. (1988), ‘A regression model for time series of counts’, *Biometrika* **75**(4), 621–629.

Zhou, Y., Wang, L., Zhang, L., Shi, L., Yang, K., He, J., Zhao, B., Overton, W., Purkayastha, S. and Song, P. (2020), ‘A spatiotemporal epidemiological prediction model to inform county-level covid-19 risk in the united states’, *Harvard Data Science Review* .

## SUPPLEMENTARY MATERIAL

**Title:** Supplement to “Robust modeling and inference of disease transmission using error-prone data with application to SARS-CoV-2”.

**R-code for Quasi-Score approach:** R-code together with part of the U.S. data used to analyze SARS-CoV-2 are available at <https://github.com/Jiasheng-Shi/Covid-Quasi-Score>. The file also contains R-codes for Bootstrap inspection for the instantaneous reproduction number estimation uncertainty.

### SECTION A: A MISCELLANY OF DISCUSSIONS, EXTENSIONS, VISUAL CONTENTS

#### A.1. Backward estimator and streamed data

During a pandemic, it’s common to estimate  $\gamma$  and  $R_t$  using streamed data. For a fixed number of time points  $N$ , an estimate of  $\gamma$ , denoted as  $\hat{\gamma}^{(N)}$ , can be obtained by iterative methods, e.g. Newton-Raphson and iteratively reweighted least squares. The estimate of  $R_t$  for the first  $N$  time points can be estimated using  $\hat{\gamma}^{(N)}$  and equation (3.4). We denote such a estimator as  $\{\hat{R}_t^{(N)}\}_{0 < t \leq N}$ , where the superscript  $N$  indicates the estimates are obtained based on data of the first  $N$  time points. When data of  $M$  new time points are collected, the estimate of  $\gamma$  can be updated using the same iterative method with  $\hat{\gamma}^{(N)}$  being the initial value. Then,  $R_t$  of the  $M$  new time points can be calculated using  $\hat{\gamma}^{(N+M)}$ , denoted as  $\{\hat{R}_t^{(N+M)}\}_{N < t \leq N+M}$ . The estimate of  $\{R_t\}_{0 < t \leq N}$  can also be updated using  $\hat{\gamma}^{(N+M)}$ , denoted as  $\{\hat{R}_t^{(N+M)}\}_{0 < t \leq N}$ . The proposed  $\{\hat{R}_t^{(N)}\}_{0 < t \leq N}$  in QSOEID algorithm is a “forward-looking” estimator for  $R_t$  (Lipsitch et al., 2020), which use data from up to and after time  $t$  to estimate  $R_t$ .

However, the procedure can also be modified to provide backward-looking estimates simply with (3.8) and (3.10) replaced by

$$\begin{aligned}\tilde{R}_t^{(k)} &= \tilde{R}_t \triangleq h^{-1} \left( \sum_{i=1}^q \theta_i f_i(D_{1,t}, D_{2,t}, \hat{D}_{3,t}) + Z_t^T \tilde{\beta}^{(t)} \right), \\ \hat{R}_k^{(k)} &= \hat{R}_k \triangleq h^{-1} \left( \sum_{i=1}^q \hat{\theta}_i^{(k)} f_i(D_{1,k}, D_{2,k}, \hat{D}_{3,k}) + Z_k^T \hat{\beta}^{(k)} \right).\end{aligned}\tag{A.1}$$

Thus backward-looking estimator for  $R_t$  uses data only from past and present. When the estimators approaching oracle parameter values, the forward-looking estimator updates the

entire  $\{R_t\}_{1 \leq t \leq N}$  sequence and may have a better accuracy. In our simulation study, we found the back-looking estimator performs similarly with much less computing time and less sensitivity to initial values. In practice, whether to use the forward-looking or the backward-looking method is a trade-off between accuracy and computational cost.

## A.2. Parameter settings of the simulation study

Table A.2: Parameter values used to generate data in simulation scenarios. In all scenarios, we set  $\beta_1 = -0.02$  and  $\beta_2 = -0.125$ . Except for scenario 6, the standard deviation of the error terms in each model is determined by  $(\text{Var}\epsilon)^{1/2} \asymp \mathbb{E}|Z_{T1}|\beta_1$ .  $Z_{t1}$  was generated from  $4.5 + (t - \frac{T}{2})/6 + \mathcal{N}(0, 9)$  in scenario 2 and generated from  $9 + (t - \frac{T}{2})/16 + \mathcal{N}(0, 9)$  in scenario 3 to avoid unrealistically large values of  $R_t$ .

Scenario 1:	$T = 120$ ,	$I_0 = 500$ ,	$\epsilon \sim N(0, 10^{-3})$ ,	$\phi_0 = 0.5$ ,	$\theta_1 = 0.7$ ,
Scenario 2:	$T = 90$ ,	$I_0 = 500$ ,	$\epsilon \sim N(0, 10^{-3})$ ,	$\phi_0 = 0.5$ ,	$\theta_1 = 0.7$ ,
Scenario 3:	$T = 200$ ,	$I_0 = 500$ ,	$\epsilon \sim N(0, 10^{-3})$ ,	$\phi_0 = 0.5$ ,	$\theta_1 = 0.7$ ,
Scenario 4:	$T = 120$ ,	$I_0 = 125$ ,	$\epsilon \sim N(0, 10^{-3})$ ,	$\phi_0 = 0.5$ ,	$\theta_1 = 0.7$ ,
Scenario 5:	$T = 120$ ,	$I_0 = 250$ ,	$\epsilon \sim N(0, 10^{-3})$ ,	$\phi_0 = 0.5$ ,	$\theta_1 = 0.7$ ,
Scenario 6:	$T = 120$ ,	$I_0 = 500$ ,	$\epsilon \sim N(0, 10^{-2})$ ,	$\phi_0 = 0.5$ ,	$\theta_1 = 0.7$ ,
Scenario 7:	$T = 120$ ,	$I_0 = 500$ ,	$\epsilon \sim t_3/10^{3/2}$ ,	$\phi_0 = 0.5$ ,	$\theta_1 = 0.7$ ,
Scenario 8:	$T = 120$ ,	$I_0 = 500$ ,	$\epsilon \sim N(0, 10^{-3})$ ,	$\phi_0 = 0.5$ ,	$\theta_1 = 0.7$ , $\beta_3 = -0.03$ ,
Scenario 9:	$T = 120$ ,	$I_0 = 500$ ,	$\epsilon \sim N(0, 10^{-3})$ ,	$\phi_0 = 0.45$ ,	$\theta_1 = 0.5$ , $\theta_2 = 0.3$ ,

The estimation algorithm was applied with a pre-estimation period of 5 days, i.e.  $\tau_0 = 5$ . Each simulation scenario was repeated over 1000 replications to calculate the evaluation statistics. The infectivity function was assumed to be the same as the density function of a gamma distribution, with mean (SD) of 7.5 (4.7) days, according to a previous epidemiological survey of the first 425 SARS-CoV-2 cases in Wuhan, China (Li et al., 2020). It suggested that the time since infection to peak infectiousness is 5 to 7 days and the entire incubation period is between 3 to 24 days. Therefore,  $\omega_s = \mathbb{P}(s-1 \leq X < s)$  for  $1 \leq s < 25$ , and  $\omega_s = 0$  for  $s \geq 25$ , where  $X \sim \Gamma(k = 2.5, \theta = 3)$ .

The two daily covariates were simulated independently to mimic the real data of temperature in Philadelphia and data of social distancing from daily cellular telephone movement, provided by Unacast (Unacast, 2021, July 1st), which measured the percent change in visits to nonessential businesses, e.g., restaurants and hair salons during March 1st and June 30th, 2020. Specifically, daily temperature were generated from a shifted

normal distribution, i.e.  $Z_{t1} \stackrel{d}{=} 5 + \left(t - \frac{T}{2}\right)/8 + \mathcal{N}(0, 9)$ , for  $t = 1, \dots, T$ . The social distancing data were generated from a uniform distribution and applied a logit transformation afterwards, i.e.  $Z_{t2} \stackrel{i.i.d.}{\sim} 2 + \text{logit}(\text{Uniform}(0, 1))$ , for  $t = 1, \dots, T$ . Additionally, in the misspecified scenarios with three covariates, the third covariate was generated from  $Z_{t3} \stackrel{d}{=} \left(t - \frac{T}{2}\right)/9 + \mathcal{N}(0, 5)$ , for  $t = 1, \dots, T$ . The variations of error terms were assumed to be small as the variation of  $\log(R)$  was small with  $R$  ranging from 0.5 to 3 and has a comparable size of the variation of covariates times their effects.

### A.3. Additional results of data application

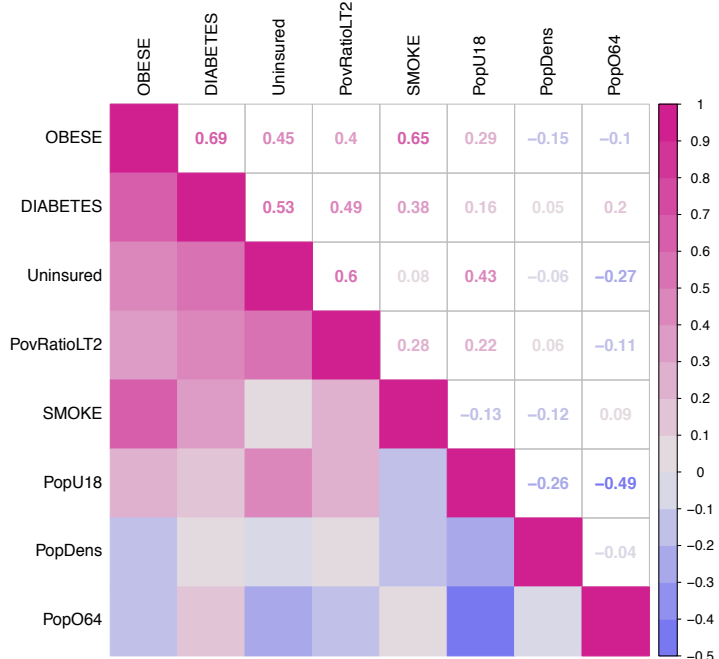


Figure A.3: Heatmap for county-level covariates; Due to high-correlation, we choose elderly population percentage from sociology related covariates and chose population percentage of diabetes from medical related covariates in the final model to avoid high correlation (correlation threshold 0.25).

Table A.3: Estimated parameter value and bootstrap interval estimator from the analysis of data from 517 US counties between February 1st and July 6th 2020 with county level case count and covariates.

$\ell$	$\alpha$	$\varrho^1$	Intercept $\phi_0$	Viscosity bet- ween daily $R_0$ , $\phi_1$	Elderly Pop. %, $\beta_1$	Pop. Density $\beta_2 (\times 10^{-2})$	Pop. Diabetes, $\beta_3$	% of Practice, $\beta_4$	Social Dist. $\beta_5 (\times 10^{-2})$	Wet-bulb Temp.
45	0.05	5	-0.511 (-0.727, 0.373)	0.708 (0.332, 0.990)	0.006 (0.005, 0.703)	-2.670 (-8.599, 0.816)	7.017 (0.136, 10.35)	0.348 (0.052, 1.222)	-1.756 (-1.367, 0.120)	
		10	-0.721 (-1.150, -0.056)	0.666 (0.194, 0.896)	2.438 (0.833, 5.633)	2.001 (-0.771, 5.373)	6.666 (1.848, 9.734)	0.608 (0.298, 1.624)	-2.209 (-2.519, -0.485)	
		15	-0.765 (-1.217, -0.065)	0.629 (0.151, 0.856)	2.660 (1.335, 5.624)	3.695 (1.639, 7.541)	7.159 (2.004, 11.43)	0.726 (0.576, 1.848)	-2.273 (-2.625, -0.443)	
	0.10	5	(-0.665, 0.303)	(0.377, 0.990)	(0.010, 0.585)	(-8.342, 0.739)	(0.153, 10.21)	(0.054, 1.142)	(-1.352, 0.063)	
		10	(-1.078, -0.068)	(0.310, 0.882)	(0.970, 5.154)	(-0.522, 4.944)	(2.006, 9.624)	(0.328, 1.404)	(-2.343, -0.539)	
		15	(-1.183, -0.077)	(0.238, 0.842)	(1.403, 5.542)	(1.745, 6.484)	(2.127, 11.19)	(0.633, 1.672)	(-2.537, -0.494)	
	0.20	5	(-0.489, 0.206)	(0.419, 0.990)	(0.022, 0.520)	(-7.165, 0.560)	(0.312, 8.742)	(0.057, 1.038)	(-1.040, 0.025)	
		10	(-1.022, -0.074)	(0.353, 0.861)	(1.166, 4.823)	(-0.400, 4.787)	(2.086, 9.426)	(0.345, 1.344)	(-1.984, -0.584)	
		15	(-1.123, -0.097)	(0.274, 0.807)	(1.600, 5.122)	(1.798, 6.375)	(2.688, 10.47)	(0.734, 1.442)	(-2.452, -0.624)	
60	0.05	5	(-0.708, 0.019)	(0.323, 0.877)	(0.033, 0.582)	(-8.659, -0.306)	(2.475, 9.922)	(0.173, 0.944)	(-1.549, -0.115)	
		10	(-1.047, -0.259)	(0.415, 0.834)	(1.476, 3.904)	(-1.945, 3.213)	(2.664, 8.220)	(0.421, 1.100)	(-2.223, -0.707)	
		15	(-1.405, -0.229)	(0.172, 0.853)	(1.330, 5.276)	(0.778, 5.790)	(2.778, 11.83)	(0.494, 1.481)	(-3.385, -0.719)	
	0.10	5	(-0.707, -0.001)	(0.369, 0.872)	(0.039, 0.537)	(-7.741, -0.608)	(2.475, 9.647)	(0.183, 0.935)	(-1.548, -0.143)	
		10	(-0.990, -0.259)	(0.433, 0.798)	(1.478, 3.897)	(-1.776, 2.797)	(2.892, 8.117)	(0.431, 1.086)	(-2.178, -0.713)	
		15	(-1.402, -0.229)	(0.180, 0.815)	(1.510, 5.274)	(0.947, 5.133)	(2.966, 11.64)	(0.549, 1.479)	(-3.366, -0.724)	
	0.20	5	(-0.634, -0.074)	(0.389, 0.851)	(0.055, 0.501)	(-7.404, -1.128)	(2.626, 9.414)	(0.198, 0.882)	(-1.417, 0.151)	
		10	(-0.933, -0.308)	(0.459, 0.790)	(1.686, 3.735)	(-1.543, 2.499)	(2.945, 8.068)	(0.507, 0.846)	(-2.113, -0.746)	
		15	(-1.349, -0.293)	(0.251, 0.804)	(1.705, 5.030)	(1.054, 4.639)	(3.031, 11.57)	(0.607, 1.471)	(-3.320, -0.729)	

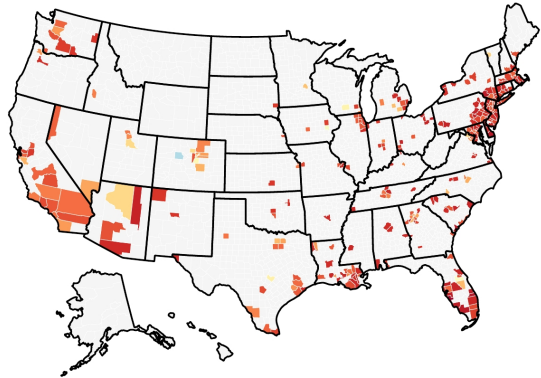
<sup>1</sup>. For  $\varrho = 5, 10$  and  $15$ , there are 516, 444, and 364 counties and 50601, 38828, and 30177 observations, respectively. Bootstrap intervals are obtained from  $k = 200$  replications.

#### A.4. Change in outbreak epicenter and evolution of the pandemic

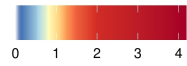
Here we present the estimated  $R_t$  of the 517 counties at six time points in Figure A.4, which demonstrated the change in outbreak epicenter and evolution of the pandemic during the study period. Each county's  $R_t$ 's were estimated using the proposed QSOEID algorithm and backward estimation.

- On April 7th, 2020, the number of counties with  $R_t$  estimated greater than 1 reached the first peak (56.3% of studied counties). We considered it as the *landmark of the early stage* of the pandemic in US. The tri-state area, together with MA and PA, constituted the main epicenter in the early stage. The virus transmission reached its peak activity in the New York state since the first case was reported. Seven of the top ten US counties that had the most accumulative cases by April 7th were in the New York state. Other counties with high transmission rate, such as the Cook county in IL, Wayne in MI and Los Angeles in CA, formed small local transmission centers with low transmission rate in their neighboring counties.
- On April 20th, 2020, the studied counties reached the *first outbreak nadir*, with most counties having  $R_t < 1$  (68.5% of studied counties) since April 7th. The quick control of transmission was mainly due to the institution of stay at home orders and broad practice of social distancing in most US states. Disease transmission in the early epicenter around the tri-state area had substantially cooled down, while daily case counts were still rising in Florida, except Broward and Miami-Dade counties.
- May 22nd, 2020, marked the *first resurgence* (second peak, 46.6% of studied counties with  $R_t > 1$ ) of COVID-19 transmission in US mainly due to the relaxation of social distancing orders. According to [The New York Times \(2020, July 28th\)](#), by May 22nd all US states that had issued stay at home orders had been at least partially reopened, except for CA, IL, WA and District of Columbia. While most states reopened around May 1st, the reopening was as early as April 20th (SC). Compared to April 20th, a new epicenter arose in the southeastern area, including TN, AL, GA, NC, SC, LA, together with FL and AR. A common characteristic shared by most counties in this new epicenter was the high percentage of population with diabetes, which may contribute to the fast disease spread. Due to the time lag between days with increased transmission and days of increased case count, regions that already cooled down with low values of  $R_t$  (Northeastern) still had more reported cases than the new epicenter (Southeastern). However, a rising epicenter would likely face a substantial increase of

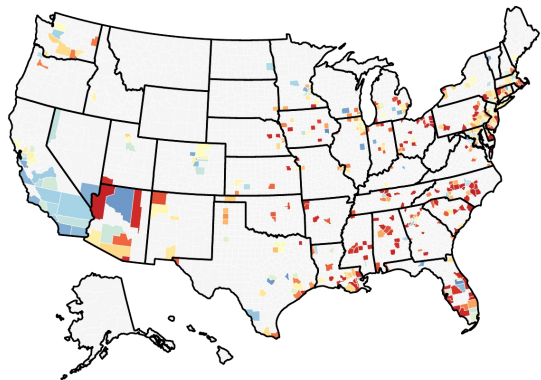
April 07th, 2020



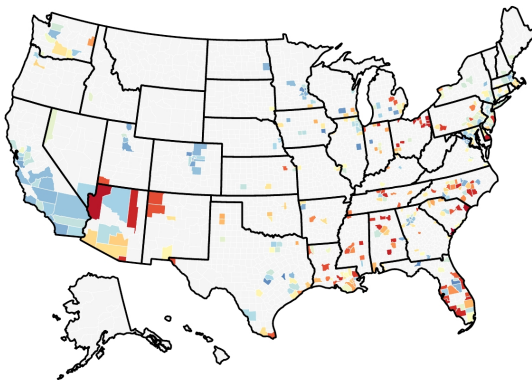
Instantaneous Reproduction Number  
April 20th, 2020,



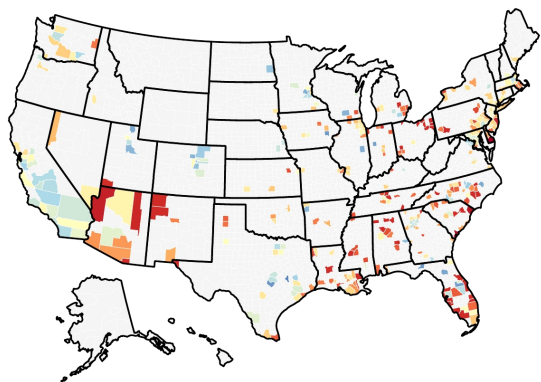
May 22nd, 2020



June 13th, 2020



June 29th, 2020



July 06th, 2020

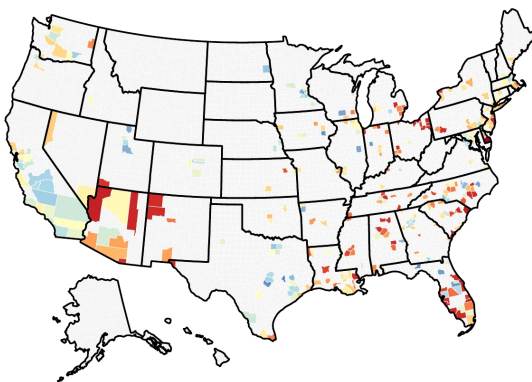


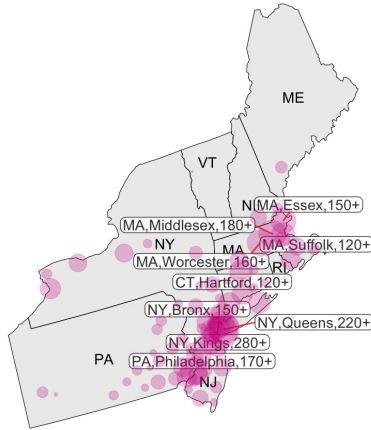
Figure A.4: Heat maps for county-level Instantaneous reproduction number around United States for selected six time points. Roughly,  $0 < R_t < 0.9$  : bluish,  $0.9 \leq R_t \leq 1.1$  : yellowish,  $R_t > 1.1$  : Reddish. The darker the blue/red, the faster the decreasing/increasing speed  $R_t$ .

Reported Cases, May 22nd

Incident Cases

100

200



Reported Cases, June 29th

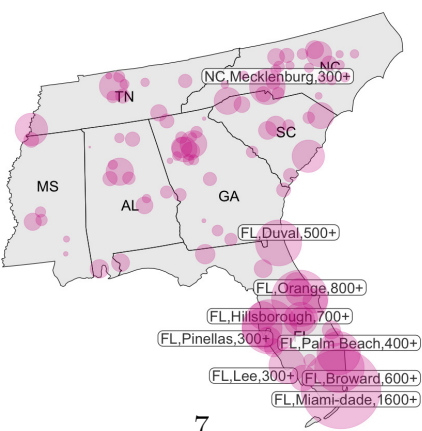


Figure A.4.1: The epicenter refer to the are with largest instantaneous reproduction number rather than having the largest daily incident cases, as shown in this picture, two areas could be different, which indicates a delay between large daily cases and high-transmission rate.

case count soon if no social distancing measures were imposed. Unfortunately, these states were all hit hard by COVID-19 in late June, as shown in Figure 5 of the main manuscript.

- It is worth to mention June 13th (second nadir, 75.8% of the reported counties having  $R_t < 1$ ) to discuss the *benefit of temperature*. Despite the small effect size, temperature played an important role in the observed decrease of COVID-19 transmission between May 22nd to June 13th. Since April 20th, the value of social distancing variable had continued to increase (indicating more activities). During the periods of April 20th - May 22nd, May 22nd - Jun 13th and Jun 13th - Jun 29th, the percentage of visits to nonessential businesses increased 22.69%, 14.73%, and 9.73%. However, the increase of daily case counts during May 22nd - Jun 13th was much slower than the other two time periods. Our model suggested that it was due to the rapid increase of wet-bulb-temperature, i.e. an increase of  $6.59^{\circ}\text{C}$  during May 22nd - Jun 13th comparing to  $4.89^{\circ}\text{C}$  and  $2.39^{\circ}\text{C}$  during April 20th - May 22nd and Jun 13th - Jun 29th.
- From June 29th to July 06th, it was when the *summer wave* hit US and new epicenters arose. With the increment of wet-bulb-temperature slowing down quickly and social distancing continuing to return back to normal, 38.1% of the studied counties had  $R > 1$  on June 29th. Different from May 22nd and June 13th, there were two epicenters. One centered around the interstate 40 westbound corridor from CA to NM, and the other one was mainly in FL (also shown in Figure 5). However, as suggested by our model, the major driving factors of the two epicenters were different, with relaxation of social distancing being the major driver in CA and higher elderly population in FL.

#### A.5. Extension to nonparametric model

The proposed method can be further extended to a nonparametric model by relaxing the assumption on link function to avoid misspecification. The estimation is straightforward if the dependency of  $\{R_t\}_{t \geq 0}$  is ignored. For example, if model assumes  $\mathbb{E}[R_t|Z_t] = f(Z_t)$  with  $\{(R_t, Z_t)\}_{t \geq 0}$  being i.i.d, then it forms a nonparametric regression problem and the function  $f(\cdot)$  can be estimated using splines regression (Friedman, 1991), wavelet regression (Hall et al., 1997), or a simple Nadaraya-Watson kernel estimator. When time series dependency of  $\{R_t\}_{t \geq 0}$  is considered, e.g.,  $\mathbb{E}[R_t|Z_t, D_{3,t}] = \phi_0 + \sum_{i=1}^q \theta_i f_i(R_{t-i}) + g(Z_t)$  with a known

$R_0$  and known functions  $f_i$ ,  $1 \leq i \leq q$  and unknown  $g(\cdot)$ , we can adopt local linear kernel estimators (Fan and Gijbels, 1996) into the proposed iterative algorithm. Define

$$\tilde{g}_{h,k+1}(z) = \frac{1}{k} \sum_{t=1}^k W_{k,t,h}(z) \left( \hat{R}_t^{(k)} - \sum_{i=1}^q \theta_i f_i(\hat{R}_{t-1}^{(k)}) - \phi_0 \right),$$

for  $k \geq \tau_0$ , where

$$\begin{aligned} W_{k,t,h}(z) &= \frac{[s_{2,k} - s_{1,k}(Z_t - z)] K_h(Z_t - z)}{s_{2,k} s_{0,k} - s_{1,k}^2}, \\ s_{r,k} &= s_{r,k}(z) = \frac{1}{k} \sum_{t=1}^k (Z_t - z)^r K_h(Z_t - z), \quad r = 0, 1, 2. \\ K_h(\cdot) &= \frac{1}{h} K(\cdot/h) \text{ satisfy } \int K_h = 1. \\ \hat{R}_t^{(\tau_0)} &\triangleq I_t / \Lambda_t, \quad \text{for } t = 1, \dots, \tau_0, \end{aligned}$$

with  $h$  being the bandwidth. Consequently, define

$$\tilde{R}_t^{(k+1)} \triangleq \phi_0 + \sum_{i=1}^q \theta_i f_i(\hat{R}_{t-1}^{(k)}) + \tilde{g}_{h,k+1}(Z_t), \quad \text{for } t = \tau_0 + 1, \dots, k + 1.$$

Updates the estimator of  $(\phi_0, \theta)$  based on the Quasi-score estimating equation,

$$\tilde{U}_{k+1}^*(\phi_0, \theta) = \sum_{t=\tau_0+1}^{k+1} \left( \frac{\partial \tilde{\mu}_t^{(k+1)}}{\partial \theta} \right)^T \left( \tilde{\nu}_t^{(k+1)} \right)^{-1} (I_t - \tilde{\mu}_t^{(k+1)}) = 0.$$

with  $\tilde{\mu}_t^{(k+1)} = \tilde{\nu}_t^{(k+1)} = \tilde{R}_t^{(k+1)} \Lambda_t$ . Or equivalently, Updates the estimator of  $(\phi_0, \theta)$  from

$$\left( \hat{\phi}_0^{(k+1)}, \hat{\theta}^{(k+1)} \right) \triangleq \arg \max_{\|\theta\|_1 < 1} \left[ \sum_{t=\tau_0+1}^{k+1} I_t \log \left( \tilde{R}_t^{(k+1)} \right) - \tilde{R}_t^{(k+1)} \Lambda_t \right], \quad (\text{A.5})$$

and obtain the estimators  $\hat{R}_t^{(k+1)}$ ,  $t = \tau_0 + 1, \dots, k + 1$  and  $\hat{g}_{h,k+1}$  by plug  $(\hat{\phi}_0^{(k+1)}, \hat{\theta}^{(k+1)})$  into the corresponding  $\tilde{R}_t^{(k+1)}$  and  $\tilde{g}_{h,k+1}$ . Furthermore, we have for  $k \geq \tau_0$  that

**Theorem 0.1 (Concavity)** (A.5) forms a globally concave maximization problem.

### A.6. Extension to random effect model

At the late period of a severe pandemic like COVID-19, the impact of herd immunity also became more evident. In order to modify the model for interactive infections and herd immunity, one of the data available for measuring between counties association is revealed by cell-phone movement across counties while we have the herd immunity level associates with region cases and region population. Those data can help divide the country into several regions, such that, between regions traveling activity level is negligible while within regions traveling activity can be modeled by a random effect, same arguments applies to herd immunity as well. So we may reformulate (3.3) as

$$\log R_{ijt} = U_i + \phi_0 + \sum_{k=1}^q \theta_k \log R_{ij,(t-k)} + Z_{ijt}^T \beta + \epsilon_{ijt},$$

where  $U_i$ ,  $1 \leq i \leq K$  is the random effect for  $K$  regions with an adapted distributional assumption  $F_U$ , and the subscript  $1 \leq i \leq K$ ,  $1 \leq j \leq n_i$ ,  $1 \leq t \leq T_0$  refer to region, county and time separately. The estimating procedure can be parallelly developed with  $\hat{R}_{js}^{(k)}$  replaced by  $(\hat{R}_{js}/e^{U_i})^{(k)}$  in (3.10) and  $\tilde{R}_{js}^{(k+1)}$  replaced by  $(\tilde{R}_{js}/e^{U_i})^{(k+1)}$  in (3.8), and most importantly, with the estimating equation replaced by

$$\begin{aligned} \frac{\partial}{\partial \theta} \tilde{\ell}_k = & \frac{\partial}{\partial \theta} \sum_{i=1}^K \int \left( \sum_{j=1}^{n_i} \sum_{s=\tau_j+1}^{\tau_j+k+1} I_{ijs} \left[ (\log \tilde{R}_{ijs} - U_i)^{(k+1)} + U_i \right] \right. \\ & \left. - \exp \left( (\log \tilde{R}_{ijs} - U_i)^{(k+1)} + U_i \right) \Lambda_{ijs} \right) dF_U(U_i) = 0. \end{aligned}$$

### A.7. Multi-counties estimation

Since structures in the proposed QSOEID algorithm are mostly additive, so for multi-counties indexed by  $j \in \{1, \dots, m\}$ , and observations for  $j$ -th county,  $(I_{js}, Z_{js})_{1 \leq s \leq T_j}$  and start instantaneous reproduction number  $R_{j0}$ , the estimation is mostly parallel. Practically, to start our iterative algorithm, pick a calendar date such that we have  $\cup_{j=1}^m \{(I_{js}, Z_{js}), 1 \leq s \leq \tau_j\}$  are observations before that specific time point. After  $k$  iterations, we use the

semi-parametric ‘‘estimator’’

$$\begin{aligned}\tilde{\beta}_{k+1} &\triangleq \left\{ \sum_{j=1}^m \sum_{s=1}^{\tau_j+k} (Z_{js} - \bar{Z}_{k+1})(Z_{js} - \bar{Z}_{k+1})^T \right\}^{-1} \\ &\quad \times \sum_{j=1}^m \sum_{s=1}^{\tau_j+k} (Z_{js} - \bar{Z}_{k+1}) \left( h(\hat{R}_{js}^{(k)}) - \sum_{i=1}^q \theta_i f_i(D_{1,s,j}, D_{2,s,j}, \hat{D}_{3,s,j}^{(k-1)}) \right),\end{aligned}$$

where  $\hat{R}_{js}^{(s)} \triangleq I_{js}/\Lambda_{js}$ ,  $1 \leq s \leq \tau_j$ ,  $1 \leq j \leq m$  is the MLE,  $\hat{R}_{js}^{(k)}$ ,  $1 \leq s \leq \tau_j + k$ ,  $1 \leq j \leq m$  is the estimator obtained in  $k$ -th iteration,  $D_{1,s,j}$ ,  $D_{2,s,j}$  and  $\hat{D}_{3,s,j}^{(k-1)}$  are defined in the way parallel to  $D_{1,s}$ ,  $D_{2,s}$  and  $\hat{D}_{3,s}^{(k-1)}$ , and

$$\bar{Z}_{k+1} = \left( \sum_{j=1}^m (\tau_j + k) \right)^{-1} \sum_{j=1}^m \sum_{s=1}^{\tau_j+k} Z_{js}.$$

For  $1 \leq j \leq m$ ,  $1 \leq s \leq \tau_j + k + 1$ , define

$$\tilde{R}_{js}^{(k+1)} \triangleq h^{-1} \left( \sum_{i=1}^q \theta_i f_i(D_{1,s,j}, D_{2,s,j}, \hat{D}_{3,s,j}^{(k-1)}) + Z_{js}^T \tilde{\beta}_{k+1} \right),$$

and update the estimator of  $\theta$  based on quasi-score equation

$$U_k(\theta) = \sum_{j=1}^m \sum_{s=\tau_j+1}^{\tau_j+k+1} \left( \frac{\partial \tilde{\mu}_{js}^{(k+1)}}{\partial \theta} \right)^T \left( \tilde{\nu}_{js}^{(k+1)} \right)^{-1} (I_{js} - \tilde{\mu}_{js}^{(k+1)}) \quad (\text{A.7})$$

where  $\tilde{\mu}_{js}^{(k+1)} = \tilde{\nu}_{js}^{(k+1)} = \tilde{R}_{js}^{(k+1)} \Lambda_{js}$  and  $\Lambda_{js}$  are similarly defined as  $\Lambda_s$  but for the  $j$ -th county. One can obtain the estimator of  $j$ -th counties instantaneous reproduction number and covariates effect size by plugin the quasi-score equation of  $\theta$  obtained from (A.7).

#### A.8. Extension to general unknown variance function $g(\cdot)$

Local polynomial fitting is one of the most common procedure for tackling the issue of unknown variance function in Quasi-score estimation procedure. Like introduced in [Chiou and Müller \(1998\)](#), we may add the local polynomial fitting of the general variance function

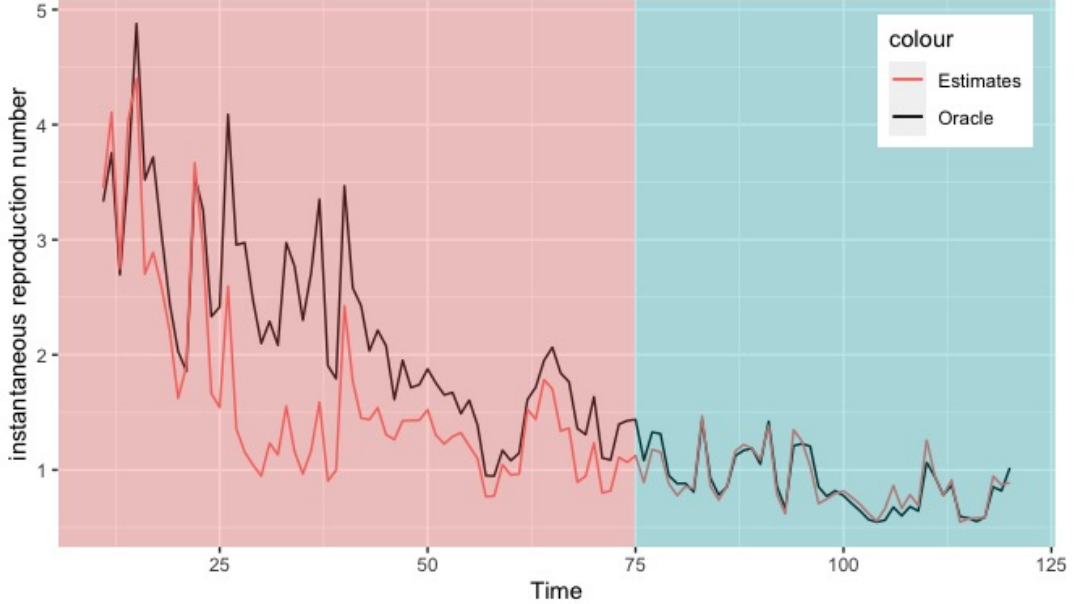


Figure A.8: The oracle instantaneous reproduction number is generated with  $\nu = g(\mu) = \sqrt{\mu}$ , while the estimated instantaneous reproduction number is estimated using identity function as the variance function  $g(\cdot)$ . The simulation result suggests that the estimation of the  $R_t$  would be rather insensitive to specification of the variance function, even for the early time period that the estimation and the oracle  $R_t$  differs a little, the estimates still captures the trend of the oracle  $R_t$ .

$g(\cdot)$  when apply the proposed quasi-score estimation procedure for multi-counties indexed by  $j \in \{1, \dots, m\}$  and observations  $\cup_{j=1}^m \{(I_{js}, Z_{js}), 1 \leq s \leq T_j\}$ .

Specifically, for a given kernel function  $K(\cdot)$  and a band width  $h$ , local polynomial fitting estimator of the  $g(\mu)$  is given by

$$\hat{g}(\mu) = \hat{a}_0(\mu),$$

where  $\hat{a}_0(\mu)$  and  $\hat{a}_1(\mu)$  minimize the weighted square-loss

$$Loss(a_0, a_1; \mu, \{\hat{\mu}_{js}\}_{1 \leq s \leq T_j}^{1 \leq j \leq m}) \triangleq \sum_{j=1}^m \sum_{s=1}^{\tau_j+k} \left[ (I_{js} - \hat{\mu}_{js})^2 - a_1(\hat{\mu}_{js} - \mu) - a_0 \right]^2 K\left(\frac{\hat{\mu}_{js} - \mu}{h}\right), \quad (A.8)$$

and  $\hat{\mu}_{js}$  is defined the same as  $\mu_{js}$  with parameter  $(\beta, \theta)$  replaced by a given pair  $(\hat{\beta}, \hat{\theta})$ .

This local polynomial fitting estimator is slightly time-consuming in our case. Notice that the loss function is defined with a given pair of parameter values  $(\hat{\beta}, \hat{\theta})$ . Hence when trying to solve the quasi-score equation (A.7) with  $\tilde{\nu} = g(\tilde{\mu})$ , we have an implicit form on the right hand side of (A.7). We may calculate  $U_k(\theta)$  for each given  $\theta$  as the the form of  $g(\cdot)$  can be obtained when  $\theta$  is given, and seeking for the zero points afterwards. But Newton-Raphson's method can't been directly applied here.

Fortunately, the applying of such a local polynomial fitting estimator might not be that necessary in our case. For many cases of quasi-score estimation involve regression and covariates, as stated in [Liang and Hanfelt \(1994\)](#), “the quasi-likelihood method appears to be insensitive to the variance specification as the  $\beta$  estimates and especially the corresponding robust standard error estimates are remarkably stable”.

A small simulation we conducted as shown in Figure [A.8](#) supports claim of [Liang and Hanfelt \(1994\)](#). The oracle instantaneous reproduction number is generated with  $\nu = g(\mu) = \sqrt{\mu}$ , while the estimated instantaneous reproduction number is estimated using identity function as the variance function  $g(\cdot)$ . The simulation result shows the overall estimation of instantaneous reproduction number is accurate especially when the sample size is increasing. Even for the early time period that the estimation and the oracle  $R_t$  differs a little, the estimates still captures the trend of the oracle  $R_t$ , suggests the insensitive of estimation when regression structure and covariates information are involved like our case.

#### A.9. Robustness comparison between TSI model and simple compartmental model

In general, though the classic epidemiological compartmental models can capture the dynamics of disease spread, as pointed out in [Quick et al. \(2021\)](#) and I quote, “are difficult to extend to flexible regression models on covariates”. Therefore, although compartment models like the classical SIR model have used the suspected cases and recovery cases data, but it involved no covariates data into the model, which turns out would costing it to be less robust than TSI model as shown in our simulation.

First, we tested our proposed QSOEID algorithm on the data generated from SIR model in the following steps:

Step 1. Generate the covariates data according to supplementary material [A.2](#).

Step 2. Generate the underlying oracle time series model using (3.3).

Step 3. Generate recovery rate  $\gamma_t$ .

Step 4. Calculating the transmission rate  $\beta_t = \gamma_t \cdot R_t$  and incident cases with a fixed initial incident case number  $I_0$  and initial recovery case number  $Rec_0$  through SIR model equations.

Step 5. Run QSOEID algorithm with the generated covariates and incident cases.

as known in Figure A.9, despite having a rough start on the estimation of the instantaneous reproduction number at the beginning, estimates based on our proposed QSOEID algorithm quickly captured the trend of  $R_t$  and presented a rather robust performance after sample size increased over 60.

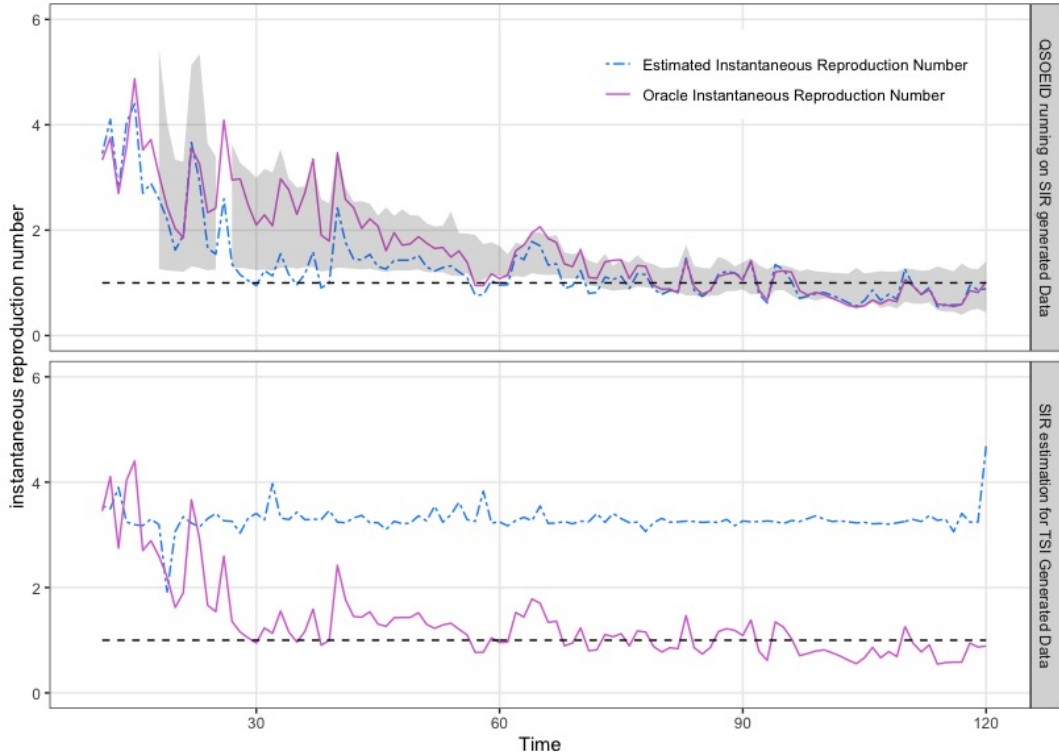


Figure A.9: Robustness comparison between TSI model and basic SIR model.

Second, we tested the SIR model estimator proposed in [Chen et al. \(2020\)](#) using the data generated from the TSI model proposed in (3.3) and  $I_t \sim Poisson(R_t \Lambda_t)$ . Specifically,

Step 1. Generate the covariates data according to supplementary material [A.2](#).

Step 2. Generate the underlying oracle time series model using (3.3).

Step 3. Generate the incident case number from  $I_t \sim Poisson(R_t \Lambda_t)$  with a initial incident case number  $I_0$  and infectiousness profile according to supplementary material A.2.

Step 4. Generate recovery rate  $\gamma_t$ .

Step 5. Calculating the transmission rate  $\beta_t = \gamma_t \cdot R_t$ .

Step 6. Estimate the transmission rate  $\beta_t$  and recovery rate  $\gamma_t$  according to [Chen et al. \(2020\)](#).

Step 7. Calculate the estimation of instantaneous reproduction number by  $\hat{R}_t = \hat{\beta}_t / \hat{\gamma}_t$ .

Unfortunately, the SIR model estimator drifts away from the oracle  $R_t$ . Possible reasons for the performance could be that there exists measurement error in the data generation process, small sample size/incident cases number, or the sensitivity of ratio structure  $\hat{R}_t = \hat{\beta}_t / \hat{\gamma}_t$  causing  $\hat{R}_t$  differs from  $R_t$ .

Overall, this small simulation suggests the proposed QSOEID algorithm would have a great robust performance even under model mis-specification cases like the data are actually generated from compartment models.

## SECTION B: ASYMPTOTIC MIXTURE NORMALITY OF QUASI-SCORE ESTIMATOR UNDER EQUATION (4.2)

It's clear that on the extinction set  $\mathcal{E}$ ,

$$\mathcal{E}_{\text{none}} = \mathcal{E}^c, \quad \text{and} \quad \mathcal{E} \triangleq \left\{ \exists K, \text{ s.t., } I_t = 0, \text{ for } t > K \right\} = \bigcup_{t \geq 1} \{\mu_t = 0\}. \quad (\text{B.1})$$

no consistent estimator  $\hat{\gamma}$  can be expected, and  $(\hat{\gamma} - \gamma_0)^T A_n (\hat{\gamma} - \gamma_0) \rightarrow \infty$  almost surely on the extinction set if  $\lambda_{\min}(A_n) \rightarrow \infty$ . Unfortunately, due to the high variability introduced by different  $R_t$  and  $x_t$ , there is no neat form for calculating the extinction probability unlike the case in Bienaym  -Galton-Watson branching process. So we simply left the extinction probability

$$\mathbb{P}(\mathcal{E}) = \mathbb{P}\left(\bigcup_{t \geq q} \{\mu_t = 0\}\right)$$

there and only focusing on the asymptotic behaviour of  $\hat{\gamma}$  on the non-extinction set  $\mathcal{E}_{\text{none}}$ .

According to theorem 3 of [Kaufmann \(1987\)](#), and assume the following condition 1,

**Condition 1** (i). *There exists some nonrandom nonsingular normalizing matrix  $A_N$ , s.t., the normalized conditional variance converge to a a.s. positive definite random matrix  $\zeta^T \zeta$ , i.e.,*

$$A_N^{-1} \left[ \sum_{t=q}^N \text{Cov}(\xi_t(\gamma_0) | \mathcal{F}_{t-1}) \right] (A_N^{-1})^T \xrightarrow{P} \zeta^T \zeta.$$

(ii). *The conditional Lindeberg condition holds, i.e., for all  $\epsilon > 0$ ,*

$$\sum_{t=q}^N \mathbb{E} \left[ \xi_t^T(\gamma_0) (A_N^T A_N)^{-1} \xi_t(\gamma_0) \cdot \mathbb{1}(|\xi_t^T(\gamma_0) (A_N^T A_N)^{-1} \xi_t(\gamma_0)| > \epsilon^2) \middle| \mathcal{F}_{t-1} \right] \xrightarrow{P} 0,$$

(iii). *The smoothness condition*

$$\sup_{\tilde{\gamma} \in \mathcal{B}_N(\delta)} \left\| A_N^{-1} \left( \frac{\partial U_N(\tilde{\gamma})}{\partial \gamma} + \sum_{t=q}^N \text{Cov}(\xi_t(\gamma_0) | \mathcal{F}_{t-1}) \right) (A_N^{-1})^T \right\| \xrightarrow{P} 0,$$

with  $\mathcal{B}_N(\delta) = \{\tilde{\gamma} : \|A_N^T(\tilde{\gamma} - \gamma_0)\| \leq \delta\}$ , holds for all  $\delta > 0$ .

we have the asymptotic normality of  $\hat{\gamma}$  under certain normalization. While the (iii) of condition 1 is hard to track and unnecessary for the special case: the embedded autocorrelated latent process (4.2), as an alternative, we propose the following condition 2. Define

$$y_t = \log(R_t) - x_t^T \beta = \log(\mu_t) - \log(\Lambda_t) - x_t^T \beta,$$

then  $\{y_t\}_{t \geq 0}$  forms a degenerated AR( $q$ ) model or a recurrence equation with order  $q$ . To avoid divergence, we require  $M = \max_t \|X_t\|_2 < \infty$  and  $\{y_t\}_{t \geq 0}$  to be causal, i.e, the roots of its characteristic polynomial are outside the unit circle.

**Condition 2** (i). *Assume (i) and (ii) of condition 1 holds for  $A_N^2 = \sum_{t=q}^N \text{Cov}(\xi_t(\gamma_0))$ .*

(ii). *Assume  $\{A_n^{-1} V_n^2(\gamma_0) (A_n^{-1})^T\}_{n \geq 1}$  defined in (B.3) is termwise uniformly integrable.*

(iii). *On  $\mathcal{E}_{\text{none}}$ , for  $\forall \gamma \in \Theta$ , the minimum eigenvalue of the normalized matrix*

$$I(\xi) \triangleq A_N^{-1} \left( -\frac{\partial U_N(\gamma)}{\partial \gamma} \Big|_{\gamma=\xi} \right) (A_N^{-1})^T$$

*is uniformly bounded away from 0, i.e,  $\exists \lambda_0 > 0$ , s.t.,  $\lambda_{\min}(I(\xi)) \geq \lambda_0$ .*

(iv). There exist some  $\phi$ , s.t,  $\|\theta(\gamma_0)\|_1 < \phi < 1$ ,  $\lim (\lambda_{\min}(A_N))^{-1} \sum_{t=q}^N \phi^{[t/q]} \mathbb{E} \mu_t < +\infty$ .

**Theorem 0.2** Under condition 2,  $\left[ \sum_{t=q}^N \text{Cov}(\xi_t(\gamma_0) | \mathcal{F}_{t-1}) \right]^{1/2} (\hat{\gamma} - \gamma_0) \xrightarrow{d} \mathcal{N}(0, I)$ .

*Proof.* (of Theorem 0.2) Without loss of generality, assume  $I_0 = 1$  and  $\{R_t, 0 \leq t < q\}$  are known. Since  $\theta_j > 0$  and  $\{y_t\}_{t \geq 0}$  is causal, so  $\|\theta\|_1 = \sum_{i=1}^q \theta_i < 1$ . By (4.2), for  $t \geq q$ ,

$$\begin{aligned} \frac{\partial \log(\mu_t)}{\partial \beta} &= x_t^T + \frac{\partial y_t}{\partial \beta}, \quad \frac{\partial y_t}{\partial \beta} = \sum_{i=1}^q \theta_i \frac{\partial y_{t-i}}{\partial \beta}, \quad \frac{\partial y_s}{\partial \beta} = -x_s^T, \quad \text{for } 0 \leq s < q, \\ \frac{\partial \log(\mu_t)}{\partial \theta} &= \frac{\partial y_t}{\partial \theta} = (y_{t-1}, \dots, y_{t-q}) + \sum_{i=1}^q \theta_i \frac{\partial y_{t-i}}{\partial \theta}, \quad \frac{\partial y_s}{\partial \theta} = 0, \quad \text{for } 0 \leq s < q. \end{aligned} \quad (\text{B.2})$$

Notice that  $R_t$ , as well as  $y_t$ , is determined when given  $\beta$  and  $\theta$ , hence  $\partial \log(\mu_t) / \partial \gamma$  is non-random when given  $\beta$  and  $\theta$ .

Recall that  $\hat{\gamma}$  is the solution of the equation  $U_N(\gamma) = 0$  and  $\gamma_0$  is the oracle parameter value. Thereby, for some  $\xi$  depends on  $\{I_t, t \geq 0\}$  and lays between  $\gamma_0$  and  $\hat{\gamma}$ , we have

$$0 = U_N(\hat{\gamma}) = U_N(\gamma_0) + \frac{\partial U_N(\gamma)}{\partial \gamma} \Big|_{\gamma=\xi} (\hat{\gamma} - \gamma_0),$$

or equivalently,

$$A_N^{-1} (T_{N,1}(\xi) + T_{N,2}(\xi) + V_N^2(\xi)) (A_N^{-1})^T A_N^T (\hat{\gamma} - \gamma_0) = A_N^{-1} U_N(\gamma_0),$$

where  $A_N^T A_N = \sum_{t=q}^N \text{Cov}(\xi_t(\gamma_0)) = \mathbb{E} V_N^2(\gamma_0)$ , so without loss of generality, we may choose  $A_N$  to be symmetric,

$$\begin{aligned} T_{N,1}(\xi) &= - \sum_{t=q}^N \frac{\partial \log(\mu_t)}{\partial \gamma \partial \gamma^T} \Big|_{\gamma=\xi} (I_t - \mu_t|_{\gamma_0}), \\ T_{N,2}(\xi) &= \sum_{t=q}^N \frac{\partial \log(\mu_t)}{\partial \gamma \partial \gamma^T} \Big|_{\gamma=\xi} (\mu_t|_{\xi} - \mu_t|_{\gamma_0}), \\ \text{and} \quad V_N^2(\xi) &= \sum_{t=q}^N \left( \frac{\partial \log(\mu_t)}{\partial \gamma} \right)^T \frac{\partial \log(\mu_t)}{\partial \gamma} \mu_t \Big|_{\gamma=\xi}. \end{aligned} \quad (\text{B.3})$$

To clear the confusion, when taking expectation or mentioning terms without specifically marked in the later paragraph, the  $I_t$  and  $\mu_t$  would always refer to the random variables generated with oracle parameters  $\gamma_0$ .

For an arbitrary given and fixed vector  $\alpha = (\alpha_1, \dots, \alpha_{p+q})^T \in \mathcal{M}_{(p+q) \times 1}$ , define

$$S_N(\alpha) \triangleq \frac{\alpha^T}{\|\alpha\|} A_N^{-1} U_N(\gamma_0) = \sum_{t=q}^N \frac{\alpha^T}{\|\alpha\|} A_N^{-1} \left( \frac{\partial \log(\mu_t)}{\partial \gamma} \right)^T (I_t - \mu_t|_{\gamma_0}) \triangleq \sum_{t=q}^N \tilde{\xi}_t.$$

It's trivial to see that  $\tilde{\xi}_t \in \mathcal{F}_t$  and  $\mathbb{E}(\tilde{\xi}_t | \mathcal{F}_{t-1}) = 0$ , hence  $\{\tilde{\xi}_t, t \geq q\}$  is a martingale difference sequence, and as one may expect, the behavior of the conditional variance

$$\tilde{V}_N^2(\alpha) \triangleq \sum_{t=q}^N \mathbb{E}(\tilde{\xi}_t^2 | \mathcal{F}_{t-1}) = \frac{\alpha^T}{\|\alpha\|} A_N^{-1} V_N^2(\gamma_0) (A_N^{-1})^T \frac{\alpha}{\|\alpha\|}$$

plays an important role and would directly affect the limiting distribution of  $S_N(\alpha)$ . Condition 2 (i) automatically ensures that there exist some random variable  $\zeta(a) = (\frac{\alpha^T}{\|\alpha\|} \zeta^T \zeta \frac{\alpha}{\|\alpha\|})^{1/2}$ , s.t.,  $\mathbb{E}\zeta^2(a) < \infty$  and

$$\tilde{V}_N^2(\alpha) \xrightarrow{P} \zeta^2(\alpha). \quad (\text{B.4})$$

Meanwhile, (ii) of condition 2 implies, for  $\forall \alpha$ ,

$$\left\{ \tilde{V}_n^2(\alpha) \right\}_{n \geq 1} \in \text{Convex} \left\{ \left( A_n^{-1} V_n^2(\gamma_0) (A_n^{-1})^T \right)_{ij}, 1 \leq i, j \leq p+q, n \geq 1 \right\}$$

is uniformly integrable, so we conclude  $\tilde{V}_N^2(\alpha) \xrightarrow{L_1} \zeta^2(\alpha)$  and  $\mathbb{E}\tilde{V}_N^2(\alpha) = \mathbb{E}\zeta^2(\alpha) = 1$ . Hence  $\mathbb{E}(\max_{t \geq q} \tilde{\xi}_t^2) \leq 1$  uniformly in  $N$ . Together with the conditional Lindeberg condition (i) in condition 2, we conclude  $\tilde{U}_N^2(\alpha) - \tilde{V}_N^2(\alpha) \xrightarrow{L_1} 0$  by theorem 2.23 of [Hall and Heyde \(2014\)](#) for  $\tilde{U}_N^2(\alpha) \triangleq \sum_{t=q}^N \tilde{\xi}_t^2$ , hence  $\tilde{U}_N^2(\alpha) \xrightarrow{L_1} \zeta^2(\alpha)$ .

Further, since

$$0 \leq \sum_{t=q}^N \mathbb{E} \left[ \tilde{\xi}_t^2 \mathbb{1}(|\tilde{\xi}_t| > \epsilon) | \mathcal{F}_{t-1} \right] \leq \tilde{V}_N^2(\alpha) = \sum_{t=q}^N \mathbb{E}[\tilde{\xi}_t^2 | \mathcal{F}_{t-1}], \quad a.s., \quad \text{for all } N \geq 1,$$

so by a variation of dominant convergence theorem (theorem 1 in [Pratt \(1960\)](#)), we have

the Conditional Lindeberg condition is equivalent to the Lindeberg condition here, i.e.,

$$\begin{aligned}
& \text{for all } \epsilon > 0, \quad \sum_{t=q}^N \mathbb{E} \left[ \tilde{\xi}_t^2 \mathbb{1}(|\tilde{\xi}_t| > \epsilon) \right] \rightarrow 0, \quad \text{which further implies} \\
& \Rightarrow \text{ for all } \epsilon > 0, \quad \sum_{t=q}^N \tilde{\xi}_t^2 \mathbb{1}(|\tilde{\xi}_t| > \epsilon) \xrightarrow{P} 0, \\
& \Leftrightarrow \text{ for all } \epsilon > 0, \quad \mathbb{P} \left( \sum_{t=q}^N \tilde{\xi}_t^2 \mathbb{1}(|\tilde{\xi}_t| > \epsilon) > \epsilon^2 \right) = \mathbb{P} \left( \max_{t \geq q} |\tilde{\xi}_t| > \epsilon \right) \rightarrow 0, \\
& \Leftrightarrow \text{ for all } \epsilon > 0, \quad \max_{t \geq q} |\tilde{\xi}_t| \xrightarrow{P} 0. \tag{B.5}
\end{aligned}$$

Combine (B.5), the fact that  $\tilde{U}_N^2(\alpha) \xrightarrow{L_1} \zeta^2(\alpha)$  and  $\mathbb{E}(\max_{t \geq q} \tilde{\xi}_t^2) \leq 1$  uniformly in  $N$ , we claim that by using the martingale central limit theorem (see e.g, theorem 3.2 of [Hall and Heyde \(2014\)](#)), for  $Z$  being a standard normal distributed random variable and being independent of  $\zeta(\alpha)$ ,

$$S_N(\alpha) \xrightarrow{d} \zeta(\alpha) \cdot Z \text{ (stably).}$$

Hence the  $A_N^{-1}U_N(\gamma_0)$  converge to certain distribution with characteristic function

$$f_{A_N^{-1}U_N(\gamma)}(\alpha) = \mathbb{E} \exp \left( i\alpha^T A_N^{-1}U_N(\gamma_0) \right) \rightarrow \mathbb{E} \exp \left( -\frac{1}{2} \|\alpha\|_2^2 \zeta^2(\alpha) \right),$$

or equivalently,

$$A_N^{-1}U_N(\gamma_0) \xrightarrow{d} \zeta^T \cdot Z \text{ (stably).} \tag{B.6}$$

for  $\zeta$  independent of  $Z \sim \mathcal{N}(0, I)$ . Of course, the limit distribution holds only on the non-extinction set  $\mathcal{E}_{\text{none}}$ . Since  $\zeta, Z$  are also measurable, so we have  $A_N^{-1}U_N(\gamma_0) \xrightarrow{P} \zeta^T \cdot Z$ .

Next, for the  $(p+q) \times (p+q)$  matrix  $\partial U_N(\gamma)/\partial \gamma$ , apparently, we have  $V_N^2(\xi)$  being non-negative definite while  $T_{N,1}(\gamma_0)$  is a martingale sequence with mean zero. According to (iii) of condition 2, for  $\forall \alpha \in \mathcal{M}_{(p+q) \times 1}$  and  $\alpha \neq 0$ ,

$$\left| \frac{\alpha^T}{\|\alpha\|} A_N(\hat{\gamma} - \gamma_0) \right| = \left| \frac{\alpha^T}{\|\alpha\|} A_N^T \left( -\frac{\partial U_N(\gamma)}{\partial \gamma} \Big|_{\gamma=\xi} \right)^{-1} A_N A_N^{-1} U_N(\gamma_0) \right| < \infty, \quad a.s. \tag{B.7}$$

Meanwhile, from (B.5), we know that conditional Lindeberg condition implies that for all  $t \geq q$  and all  $\alpha$ ,

$$\frac{\alpha^T}{\|\alpha\|} A_N^{-1} \left( \frac{\partial \log(\mu_t)}{\partial \gamma} \right)^T \left( \frac{\partial \log(\mu_t)}{\partial \gamma} \right) \Big|_{\gamma=\gamma_0} (A_N^{-1})^T \frac{\alpha}{\|\alpha\|} \mu_t \xrightarrow{P} 0. \tag{B.8}$$

$V_N^2(\gamma_0)$  being positive definite for large  $N$  implies that on the non-extinction set, there exists  $\{k_1, \dots, k_q\}$  such that  $\{\partial \log(\mu_t)/\partial \gamma, t \in \{k_1, \dots, k_q\}\}$  are linear independent, combine with (B.8) concludes that the minimum eigenvalue of  $A_N$  increase to infinity, denote as  $\lambda_{\min}(A_N) \rightarrow +\infty$ . Thus (B.7) implies  $\hat{\gamma} - \gamma_0 \xrightarrow{P} 0$ .

Based on (B.2), we have

$$\begin{aligned} \frac{\partial \log(\mu_t)}{\partial \beta \partial \beta^T} &= 0, \quad \frac{\partial \log(\mu_t)}{\partial \beta \partial \theta^T} = \left( \left( \frac{\partial y_{t-1}}{\partial \beta} \right)^T, \dots, \left( \frac{\partial y_{t-q}}{\partial \beta} \right)^T \right) + \sum_{i=1}^q \theta_i \frac{\partial y_{t-i}}{\partial \beta \partial \theta^T}, \\ \frac{\partial \log(\mu_t)}{\partial \theta \partial \theta^T} &= \frac{\partial y_t}{\partial \theta \partial \theta^T} = 2 \left( \left( \frac{\partial y_{t-1}}{\partial \theta} \right)^T, \dots, \left( \frac{\partial y_{t-q}}{\partial \theta} \right)^T \right)^T + \sum_{i=1}^q \theta_i \frac{\partial y_{t-i}}{\partial \theta \partial \theta^T}. \end{aligned} \quad (\text{B.9})$$

By denote the bound of the first  $q$  terms of  $y_t|_{\gamma_0}$  and  $\partial y_t/\partial \beta_j|_{\gamma_0}$ ,  $1 \leq j \leq p$ , as  $\tilde{M}$ , then it's straightforward to see from induction that for all  $t$ ,

$$\left| \frac{\partial y_t}{\partial \beta_j} \Big|_{\gamma_0} \right| \leq \|\theta(\gamma_0)\|_1^{[t/q]} \tilde{M}, \quad 1 \leq j \leq p, \quad \text{and} \quad \left| y_t \Big|_{\gamma_0} \right| \leq \|\theta(\gamma_0)\|_1^{[t/q]} \tilde{M}$$

Here,  $[\cdot]$  denotes the floor function. Since  $\|\theta(\gamma_0)\|_1 < 1$ , define

$$\tilde{M}' = \frac{\tilde{M}/\|\theta(\gamma_0)\|_1}{\phi - \|\theta(\gamma_0)\|_1} + \max_{1 \leq i \leq q, 0 \leq t < q} \left\{ \left| \frac{\partial y_t}{\partial \theta_i} \Big|_{\gamma_0} \right| \right\},$$

so for  $1 \leq i \leq q$ , we have

$$\begin{aligned} \left| \frac{\partial y_t}{\partial \theta_i} \Big|_{\gamma_0} \right| &= \left| y_{t-i} \Big|_{\gamma_0} + \sum_{s=1}^q \theta_s \frac{\partial y_{t-s}}{\partial \theta_i} \Big|_{\gamma_0} \right| \leq \left| y_{t-i} \Big|_{\gamma_0} \right| + \|\theta(\gamma_0)\|_1 \max_{1 \leq s \leq q} \left\{ \left| \frac{\partial y_{t-s}}{\partial \theta_i} \Big|_{\gamma_0} \right| \right\} \\ &\leq \|\theta(\gamma_0)\|_1^{1+[t-i]/q} \frac{\tilde{M}}{\|\theta(\gamma_0)\|_1} + \|\theta(\gamma_0)\|_1 \max_{1 \leq s \leq q} \left\{ \left| \frac{\partial y_{t-s}}{\partial \theta_i} \Big|_{\gamma_0} \right| \right\} \\ &\leq (\phi - \|\theta(\gamma_0)\|_1) \phi^{[t/q]} \tilde{M}' + \|\theta(\gamma_0)\|_1 \max_{1 \leq s \leq q} \left\{ \left| \frac{\partial y_{t-s}}{\partial \theta_i} \Big|_{\gamma_0} \right| \right\} \end{aligned}$$

then it's straightforward to see from induction that for all  $t$ ,

$$\left| \frac{\partial y_t}{\partial \theta_i} \Big|_{\gamma_0} \right| \leq \phi^{[t/q]} \tilde{M}', \quad 1 \leq i \leq q.$$

Now, for  $0 \leq t < q$ , it's obvious from (4.2) and (B.2) that

$$\begin{aligned} \left| \frac{\partial y_t}{\partial \beta_j} \Big|_{\xi} - \frac{\partial y_t}{\partial \beta_j} \Big|_{\gamma_0} \right| &= 0 \leq \phi^{[t/q]} M \cdot \sqrt{q} \|\xi - \gamma_0\|_2, \quad \text{for } 1 \leq j \leq p, \\ \left| \frac{\partial y_t}{\partial \theta_i} \Big|_{\xi} - \frac{\partial y_t}{\partial \theta_i} \Big|_{\gamma_0} \right| &= 0 \leq \phi^{[t/q]} M' \cdot \sqrt{q} \|\xi - \gamma_0\|_2, \quad \text{for } 1 \leq i \leq q, \\ \left| y_t \Big|_{\xi} - y_t \Big|_{\gamma_0} \right| &\leq \phi^{[t/q]} M \cdot \sqrt{q} \|\xi - \gamma_0\|_2, \end{aligned} \tag{B.10}$$

for finite

$$M = \max \left\{ \frac{3\tilde{M}}{\phi - \|\theta(\gamma_0)\|_1}, \|x_t\|_2, t \geq 0 \right\}, \quad \text{and} \quad M' = \frac{3(\tilde{M}' + M)}{\phi - \|\theta(\gamma_0)\|_1}.$$

Suppose (B.10) holds for all  $0 \leq t < k$ , then for  $t = k$  and  $\sqrt{q} \|\xi - \gamma_0\|_2 < (\phi - \|\theta(\gamma_0)\|_1)/3$ , which will be the case for large  $N$  and with high probability since  $\xi$  lays between  $\gamma_0$  and its consistent estimator  $\hat{\gamma}$ ,

$$\begin{aligned} \left| \frac{\partial y_k}{\partial \beta_j} \Big|_{\xi} - \frac{\partial y_k}{\partial \beta_j} \Big|_{\gamma_0} \right| &= \left| \sum_{i=1}^q \left( \theta_i \frac{\partial y_{k-i}}{\partial \beta_j} \right) \Big|_{\xi} - \sum_{i=1}^q \left( \theta_i \frac{\partial y_{k-i}}{\partial \beta_j} \right) \Big|_{\gamma_0} \right| \\ &\leq \left| \sum_{i=1}^q \left( \theta_{i,\xi} - \theta_{i,\gamma_0} \right) \left( \frac{\partial y_{k-i}}{\partial \beta_j} \Big|_{\xi} - \frac{\partial y_{k-i}}{\partial \beta_j} \Big|_{\gamma_0} \right) \right| + \left| \sum_{i=1}^q \theta_{i,\gamma_0} \left( \frac{\partial y_{k-i}}{\partial \beta_j} \Big|_{\xi} - \frac{\partial y_{k-i}}{\partial \beta_j} \Big|_{\gamma_0} \right) \right| \\ &\quad + \left| \sum_{i=1}^q \left( \theta_{i,\xi} - \theta_{i,\gamma_0} \right) \frac{\partial y_{k-i}}{\partial \beta_j} \Big|_{\gamma_0} \right| \\ &\leq \left| \sum_{i=1}^q \left( \theta_{i,\xi} - \theta_{i,\gamma_0} \right) \right| \cdot \phi^{[k/q]-1} M \sqrt{q} \|\xi - \gamma_0\|_2 + \left| \sum_{i=1}^q \theta_{i,\gamma_0} \right| \cdot \phi^{[k/q]-1} M \sqrt{q} \|\xi - \gamma_0\|_2 \\ &\quad + \left| \sum_{i=1}^q \left( \theta_{i,\xi} - \theta_{i,\gamma_0} \right) \right| \cdot \|\theta(\gamma_0)\|_1^{[k/q]-1} \tilde{M} \leq \phi^{[k/q]} M \cdot \sqrt{q} \|\xi - \gamma_0\|_2 \end{aligned}$$

holds for  $1 \leq j \leq p$ , and similarly, we have

$$\left| y_k \Big|_{\xi} - y_k \Big|_{\gamma_0} \right| \leq \phi^{[k/q]} M \cdot \sqrt{q} \|\xi - \gamma_0\|_2.$$

Correspondingly, for  $1 \leq i \leq q$ ,

$$\begin{aligned}
\left| \frac{\partial y_k}{\partial \theta_i} \Big|_{\xi} - \frac{\partial y_k}{\partial \theta_i} \Big|_{\gamma_0} \right| &\leq \left| y_{k-i} \Big|_{\xi} - y_{k-i} \Big|_{\gamma_0} \right| + \left| \sum_{s=1}^q \left( \theta_s \frac{\partial y_{k-s}}{\partial \theta_i} \right) \Big|_{\xi} - \sum_{s=1}^q \left( \theta_s \frac{\partial y_{k-s}}{\partial \theta_i} \right) \Big|_{\gamma_0} \right| \\
&\leq \left| \sum_{s=1}^q \left( \theta_{s,\xi} - \theta_{s,\gamma_0} \right) \right| \cdot \phi^{[k/q]-1} M' \sqrt{q} \|\xi - \gamma_0\|_2 + \left| \sum_{s=1}^q \theta_{s,\gamma_0} \right| \cdot \phi^{[k/q]-1} M' \sqrt{q} \|\xi - \gamma_0\|_2 \\
&\quad + \left| \sum_{s=1}^q \left( \theta_{s,\xi} - \theta_{s,\gamma_0} \right) \right| \cdot \phi^{[k/q]-1} \tilde{M}' + \phi^{[(k-i)/q]} M \sqrt{q} \|\xi - \gamma_0\|_2 \leq \phi^{[k/q]} M' \cdot \sqrt{q} \|\xi - \gamma_0\|_2
\end{aligned}$$

Hence by induction that (B.10) holds for all  $t \geq 0$ . Similarly, we may use induction to conclude that

$$\begin{aligned}
\left| \frac{\partial \log(\mu_t)}{\partial \beta_j \partial \theta_{i_1}} \Big|_{\gamma_0} \right| &\leq \phi^{[t/q]} \tilde{M}'', \quad \left| \frac{\partial \log(\mu_t)}{\partial \beta_j \partial \theta_{i_1}} \Big|_{\xi} - \frac{\partial \log(\mu_t)}{\partial \beta_j \partial \theta_{i_1}} \Big|_{\gamma_0} \right| \leq \phi^{[k/q]} M'' \cdot \sqrt{q} \|\xi - \gamma_0\|_2, \\
\left| \frac{\partial \log(\mu_t)}{\partial \theta_{i_1} \partial \theta_{i_2}} \Big|_{\gamma_0} \right| &\leq \phi^{[t/q]} \tilde{M}'', \quad \left| \frac{\partial \log(\mu_t)}{\partial \theta_{i_1} \partial \theta_{i_2}} \Big|_{\xi} - \frac{\partial \log(\mu_t)}{\partial \theta_{i_1} \partial \theta_{i_2}} \Big|_{\gamma_0} \right| \leq \phi^{[k/q]} M'' \cdot \sqrt{q} \|\xi - \gamma_0\|_2, \quad (\text{B.11})
\end{aligned}$$

for  $1 \leq j \leq p$ ,  $1 \leq i_1, i_2 \leq q$  and some constants  $M'', \tilde{M}''$  depends on  $\|\theta(\gamma_0)\|_1$  but not  $t$ .

Since  $A_N^T A_N$  is symmetric and positive definite, so there exist a orthonormal matrix  $P$  such that  $A_N^T A_N = P^T \Lambda P$ , where  $\Lambda = \text{diag}(\lambda_1, \dots, \lambda_{p+q})$  with  $|\lambda_{p+q}| \geq \dots \geq |\lambda_1|$ . Accordingly, we may choose a symmetric  $A_N$  such that  $A_N^{-1} = P^T \Lambda^{-1/2} P$ , by denote the Frobenius norm as  $\|\cdot\|_F$ , we have

$$\begin{aligned}
&\|A_N^{-1} (T_{N,1}(\xi) - T_{N,1}(\gamma_0)) (A_N^{-1})^T\|_F \\
&\leq \sum_{t=q}^N \|\Lambda^{-1/2}\|_F^2 \cdot \|P\|_F^4 \cdot \left\| \frac{\partial \log(\mu_t)}{\partial \gamma \partial \gamma^T} \Big|_{\gamma_0} - \frac{\partial \log(\mu_t)}{\partial \gamma \partial \gamma^T} \Big|_{\xi} \right\|_F \cdot \|I_t - \mu_t\|_{\gamma_0} \\
&\leq \sum_{t=q}^N \left( \sum_{k=1}^{p+q} \frac{1}{\lambda_k} \right) \cdot (p+q)^2 \cdot \sqrt{2pq + q^2} \max_{\substack{1 \leq k \leq (p+q), \\ 1 \leq i \leq q}} \left| \frac{\partial \log(\mu_t)}{\partial \gamma_k \partial \theta_i} \Big|_{\xi} - \frac{\partial \log(\mu_t)}{\partial \gamma_k \partial \theta_i} \Big|_{\gamma_0} \right| \cdot \|I_t - \mu_t\|_{\gamma_0} \\
&\leq (p+q)^3 \left( \sum_{k=1}^{p+q} \frac{1}{\lambda_k} \right) \sum_{t=q}^N \phi^{[t/q]} M'' \cdot \sqrt{q} \|\hat{\gamma} - \gamma_0\|_2 (I_t + \mu_t|_{\gamma_0}). \quad (\text{B.12})
\end{aligned}$$

So under the (iv) of condition 2, we have, for  $\forall \epsilon > 0$ ,

$$\begin{aligned}
& \mathbb{P}\left(\left\|A_N^{-1}\left(T_{N,1}(\xi) - T_{N,1}(\gamma_0)\right)(A_N^{-1})^T\right\|_F > \epsilon\right) \\
& \leq \mathbb{P}\left(\|\hat{\gamma} - \gamma_0\|_2 \cdot (\lambda_{\min}(A_N))^{-1} \sum_{t=q}^N \phi^{[t/q]}(I_t + \mu_t) > \frac{\epsilon}{\sqrt{q}(p+q)^4 M''}\right) \\
& \leq \mathbb{P}\left(\|\hat{\gamma} - \gamma_0\|_2 > \delta\right) + \frac{2\delta\sqrt{q}(p+q)^4 M''}{\epsilon} (\lambda_{\min}(A_N))^{-1} \sum_{t=q}^N \phi^{[t/q]} \mathbb{E}\mu_t \rightarrow 0
\end{aligned} \tag{B.13}$$

by let  $\delta$  goes to 0 and  $N$  goes to  $\infty$ . Hence

$$A_N^{-1}(T_{N,1}(\xi) - T_{N,1}(\gamma_0))(A_N^{-1})^T \xrightarrow{P} 0_{(p+q) \times (p+q)}. \tag{B.14}$$

Meanwhile, under the event  $\{\|\hat{\gamma} - \gamma_0\|_2 \leq \delta\}$  for some  $\delta \leq 1$ ,

$$\left| \log \left[ \frac{R_t(\xi)}{R_t(\gamma_0)} \right] \right| \leq \left| y_t|_{\xi} - y_t|_{\gamma_0} \right| + \|x_t\|_2 \cdot \|\beta|_{\xi} - \beta|_{\gamma_0}\| \leq (1 + \sqrt{q})\delta M$$

hence

$$\left| \frac{R_t(\xi)}{R_t(\gamma_0)} - 1 \right| \leq \exp \left[ (1 + \sqrt{q})M \right] (1 + \sqrt{q})M\delta \triangleq \bar{M}\delta. \tag{B.15}$$

On one hand, if we define an intermediate term  $V_{N,int}^2$  as

$$V_{N,int}^2 = \sum_{t=q}^N \left( \frac{\partial \log(\mu_t)}{\partial \gamma} \right)^T \frac{\partial \log(\mu_t)}{\partial \gamma} \Big|_{\gamma_0} \cdot \mu_t \Big|_{\gamma=\xi},$$

then

$$\left\| A_N^{-1} \left( V_{N,int}^2 - V_N^2(\gamma_0) \right) (A_N^{-1})^T \right\|_F \leq \bar{M}\delta \cdot \left\| A_N^{-1} V_N^2(\gamma_0) (A_N^{-1})^T \right\|_F,$$

which leads to

$$\begin{aligned}
& \mathbb{P}\left(\left\| A_N^{-1} \left( V_{N,int}^2 - V_N^2(\gamma_0) \right) (A_N^{-1})^T \right\|_F > \frac{\epsilon}{2}\right) \leq \mathbb{P}\left(\bar{M}\delta \cdot \left\| A_N^{-1} V_N^2(\gamma_0) (A_N^{-1})^T \right\|_F > \frac{\epsilon}{2}\right) \\
& \leq \mathbb{P}\left(\bar{M}\delta \cdot (\|\zeta^T \zeta\|_F + 1) > \frac{\epsilon}{2}\right) + \mathbb{P}\left(\|\zeta^T \zeta\|_F + 1 < \left\| A_N^{-1} V_N^2(\gamma_0) (A_N^{-1})^T \right\|_F\right) \rightarrow 0,
\end{aligned} \tag{B.16}$$

by let  $\delta$  goes to 0 and  $N$  goes to  $\infty$ . On the other hand, similar to (B.12), we have

$$\begin{aligned}
& \|A_N^{-1} \left( V_N^2(\xi) - V_{N,int}^2 \right) (A_N^{-1})^T\|_F \\
& \leq \|\Lambda^{-1/2}\|_F^2 \cdot \|P\|_F^4 \cdot \max_{q \leq t \leq N} \left| \frac{R_t(\xi)}{R_t(\gamma_0)} \right| \cdot \left\| \sum_{t=q}^N \left[ \left( \frac{\partial \log(\mu_t)}{\partial \gamma} \right)^T \left( \frac{\partial \log(\mu_t)}{\partial \gamma} \right) \Big|_{\gamma=\gamma_0} \right. \right. \\
& \quad \left. \left. - \left( \frac{\partial \log(\mu_t)}{\partial \gamma} \right)^T \left( \frac{\partial \log(\mu_t)}{\partial \gamma} \right) \Big|_{\gamma=\xi} \right] \cdot \mu_t \Big|_{\gamma_0} \right\|_F \\
& \leq (p+q)^3 \left( \sum_{k=1}^{p+q} \frac{1}{\lambda_k} \right) \sum_{t=q}^N \phi^{[t/q]} \bar{M}' \cdot \sqrt{q} \|\hat{\gamma} - \gamma_0\|_2 \cdot \mu_t \Big|_{\gamma_0}
\end{aligned}$$

for some constant  $\bar{M}'$  depends on  $\|\theta(\gamma_0)\|_1$  but not  $t$  nor  $N$ . Thereby, same as (B.13), we have

$$\mathbb{P} \left( \|A_N^{-1} \left( V_N^2(\xi) - V_{N,int}^2 \right) (A_N^{-1})^T\|_F > \frac{\epsilon}{2} \right) \rightarrow 0, \quad (\text{B.17})$$

for which combine with (B.16) would leads us to

$$A_N^{-1} \left( V_N^2(\xi) - V_N^2(\gamma_0) \right) (A_N^{-1})^T \xrightarrow{P} 0_{(p+q) \times (p+q)}. \quad (\text{B.18})$$

Besides, it's obvious that for  $\forall \alpha \in \mathcal{M}_{(p+q) \times 1}$ ,

$$\begin{aligned}
& \frac{\alpha^T}{\|\alpha\|} A_N^{-1} T_{N,1}(\gamma_0) (A_N^{-1})^T \frac{\alpha}{\|\alpha\|} \\
& = - \sum_{t=q}^N \frac{\alpha^T}{\|\alpha\|} A_N^{-1} \frac{\partial \log(\mu_t)}{\partial \gamma \partial \gamma^T} \Big|_{\gamma=\gamma_0} (A_N^{-1})^T \frac{\alpha}{\|\alpha\|} (I_t - \mu_t) \triangleq \sum_{t=q}^N \tilde{b}_t (I_t - \mu_t)
\end{aligned}$$

is a martingale sequence, with

$$\begin{aligned}
|\tilde{b}_t| & \leq \frac{\|\alpha\|_F^2}{\|\alpha\|_2^2} \cdot \|\Lambda^{-1/2}\|_F^2 \cdot \|P\|_F^4 \cdot \sqrt{2pq + q^2} \max_{\substack{1 \leq k \leq (p+q), \\ 1 \leq i \leq q}} \left| \frac{\partial \log(\mu_t)}{\partial \gamma_k \partial \theta_i} \Big|_{\gamma_0} \right| \\
& \leq (p+q)^3 \left( \sum_{k=1}^{p+q} \frac{1}{\lambda_k} \right) \phi^{[t/q]} \tilde{M}''.
\end{aligned} \quad (\text{B.19})$$

Hence from (iv) of condition 2,

$$\begin{aligned} \mathbb{E} \left[ \sum_{t=q}^N \tilde{b}_t (I_t - \mu_t) \right]^2 &\leq \sum_{t=q}^N |\tilde{b}_t|^2 \cdot \mathbb{E} (I_t - \mu_t)^2 \\ &\leq (p+q)^8 \tilde{M}''^2 (\lambda_{\min}(A_N))^{-2} \sum_{t=q}^N \phi^{[t/q]} \mathbb{E} \mu_t \rightarrow 0, \end{aligned}$$

and by Chebyshev's inequality that  $(\alpha^T / \|\alpha\|) A_N^{-1} T_{N,1}(\gamma_0) (A_N^{-1})^T (\alpha / \|\alpha\|) \rightarrow_p 0$ , and since  $\alpha$  is arbitrary, so it's equivalent to say

$$A_N^{-1} T_{N,1}(\gamma_0) (A_N^{-1})^T \xrightarrow{P} 0_{(p+q) \times (p+q)}. \quad (\text{B.20})$$

For the last term which relates to  $T_{N,2}(\xi)$ , we introduce an intermediate  $T_{N,int}$  defined as

$$T_{N,int} = \sum_{t=q}^N \frac{\partial \log(\mu_t)}{\partial \gamma \partial \gamma^T} \Big|_{\gamma=\gamma_0} (\mu_t|_\xi - \mu_t|_{\gamma_0}),$$

then similar to (B.12), we may derive

$$\begin{aligned} &\| A_N^{-1} (T_{N,2}(\xi) - T_{N,int}) (A_N^{-1})^T \|_F \\ &\leq \|\Lambda^{-1/2}\|_F^2 \cdot \|P\|_F^4 \cdot \max_{q \leq t \leq N} \left| \frac{R_t(\xi)}{R_t(\gamma_0)} - 1 \right| \cdot \left\| \sum_{t=q}^N \left[ \frac{\partial \log(\mu_t)}{\partial \gamma \partial \gamma^T} \Big|_{\gamma=\gamma_0} - \frac{\partial \log(\mu_t)}{\partial \gamma \partial \gamma^T} \Big|_{\gamma=\xi} \right] \cdot \mu_t|_{\gamma_0} \right\|_F \\ &\leq (p+q)^3 \left( \sum_{k=1}^{p+q} \frac{1}{\lambda_k} \right) \sum_{t=q}^N \phi^{[t/q]} \bar{M}' \cdot \sqrt{q} \|\hat{\gamma} - \gamma_0\|_2^2 \cdot \mu_t|_{\gamma_0} \end{aligned}$$

so same as (B.13), we conclude

$$A_N^{-1} (T_{N,2}(\xi) - T_{N,int}) (A_N^{-1})^T \xrightarrow{P} 0_{(p+q) \times (p+q)}. \quad (\text{B.21})$$

while for  $A_N^{-1} T_{N,int} (A_N^{-1})^T$ , we again consider its one-dimensional counterpart. For  $\forall \alpha \in \mathcal{M}_{(p+q) \times 1}$ , and under the event  $\{\|\hat{\gamma} - \gamma_0\|_2 \leq \delta\}$  for some  $\delta \leq 1$ , we have

$$\left| \frac{\alpha^T}{\|\alpha\|} A_N^{-1} T_{N,int} (A_N^{-1})^T \frac{\alpha}{\|\alpha\|} \right| = \left| \sum_{t=q}^N \tilde{b}_t \left[ \frac{R_t(\xi)}{R_t(\gamma_0)} - 1 \right] \mu_t|_{\gamma_0} \right| \leq \bar{M} \delta \sum_{t=q}^N |\tilde{b}_t| \cdot \mu_t|_{\gamma_0}.$$

Using (B.19) and we obtain

$$\begin{aligned}
& \mathbb{P} \left( \left| \frac{\alpha^T}{\|\alpha\|} A_N^{-1} T_{N,int} (A_N^{-1})^T \frac{\alpha}{\|\alpha\|} \right| > \epsilon \right) \\
& \leq \mathbb{P} \left( \|\hat{\gamma} - \gamma_0\|_2 > \delta \right) + \mathbb{P} \left( \bar{M} \delta \sum_{t=q}^N |\tilde{b}_t| \cdot \mu_t|_{\gamma_0} > \epsilon \right) \\
& \leq \mathbb{P} \left( \|\hat{\gamma} - \gamma_0\|_2 > \delta \right) + \frac{\bar{M} \delta \sum_{t=q}^N |\tilde{b}_t| \cdot \mathbb{E} \mu_t}{\epsilon} \\
& \leq \mathbb{P} \left( \|\hat{\gamma} - \gamma_0\|_2 > \delta \right) + \frac{\bar{M} \delta}{\epsilon} \cdot (p+q)^4 \tilde{M}'' (\lambda_{\min}(A_N))^{-1} \sum_{t=q}^N \phi^{[t/q]} \mathbb{E} \mu_t \rightarrow 0
\end{aligned}$$

by let  $\delta$  goes to 0 and  $N$  goes to  $\infty$ . Also, since  $\alpha$  is arbitrary, so it's equivalent to say that

$$A_N^{-1} T_{N,int} (A_N^{-1})^T \xrightarrow{P} 0_{(p+q) \times (p+q)}. \quad (\text{B.22})$$

Overall, combine (B.14), (B.18) and (B.20)-(B.22), and the (i) of condition 2 that  $\tilde{V}_N^2 = A_N^{-1} V_N^2(\gamma_0) (A_N^{-1})^T \xrightarrow{P} \zeta^T \zeta$ , implies

$$A_N^{-1} \left( -\frac{\partial U_N(\gamma)}{\partial \gamma} \Big|_{\gamma=\xi} \right) (A_N^{-1})^T \xrightarrow{P} \zeta^T \zeta. \quad (\text{B.23})$$

Thus, by (B.6) and (B.23), we conclude that,

$$\zeta A_N^T (\hat{\gamma} - \gamma_0) \xrightarrow{P} Z \quad (\text{B.24})$$

on the non-extinction set  $\mathcal{E}_{none}$  with  $\zeta$  being independent of  $Z \sim \mathcal{N}(0, I)$ , and since we have chosen  $\zeta$  and  $A_N$  to be symmetric, so we may also choose a symmetric matrix

$$\zeta A_N^T \left[ \sum_{t=q}^N \text{Cov}(\xi_t(\gamma_0) | \mathcal{F}_{t-1}) \right]^{-1/2} \rightarrow I \quad (\text{B.25})$$

thus we may completes the proof and obtain (4.1) by plug (B.25) into (B.24). Last, one thing worth mention is, the  $\tilde{V}_N(\alpha) - 1 = \sum b_t(I_t - \mu_t)$  can be written into a martingale difference array in this very special case, so (i) of condition 1 could be replaced by some other “martingale array convergence condition”. However, only little work has been done towards this end and seems like neither the condition in [Ghosal and Chandra \(1998\)](#) (for complete convergence) or the one in [Atchadé \(2009\)](#) is easy tracking, but it would certainly be interesting to see if one could reduce (i) of condition 1.  $\blacksquare$ .

## SECTION C: PROOFS OF THEOREM IN SECTION 4.2

*Proof. (of Theorem 4.2)* Since  $\tilde{\beta}^{(k)}$ , as well as  $\log \tilde{R}_t^{(k)}$ ,  $t = \tau_0 + 1, \dots, k$  are linear functions of  $\theta$ , so there exists constants  $a_t, b_t \in \mathbb{R}$ ,  $c_t \in \mathcal{M}_{q \times 1}$  depend on  $\mathcal{F}_{k-1}$  such that

$$\log \tilde{R}_t^{(k)} = a_t + b_t \phi_0 + c_t^T \theta, \quad \text{for } t = \tau_0 + 1, \dots, k.$$

Consequently, by plug it into the right hand side of (4.3), we obtain the profile likelihood

$$\tilde{\ell}_k = \sum_{t=\tau_0+1}^k I_t(a_t + b_t \phi_0 + c_t^T \theta) - e^{(a_t + b_t \phi_0 + c_t^T \theta)} \Lambda_t,$$

and the Hessian matrix of  $\tilde{\ell}_k$  with respect to  $\theta' = (\phi_0, \theta)$  is

$$H_k = \frac{\partial^2 \tilde{\ell}_k}{\partial \theta' \partial \theta'^T} = - \sum_{t=\tau_0+1}^k \tilde{R}_t^{(k)} \Lambda_t \begin{pmatrix} b_t \\ c_t \end{pmatrix} \begin{pmatrix} b_t & c_t^T \end{pmatrix} \leq 0.$$

Hence (4.3) is a globle concave maximization problem.  $\blacksquare$ .

*Proof. (of Theorem 7.1)* Due to the fact that  $\tilde{R}_t^{(k)}$  and  $\tilde{g}_{h,k}$  are linear functions of  $\phi_0$  and  $\theta$ , so it follows the same manner of the proof of theorem 4.2. There exists constants  $(a_t, b_t, c_t)$  depend on  $\mathcal{F}_{t-1}$  such that

$$\tilde{R}_t^{(k)} = a_t + b_t \phi_0 + c_t^T \theta, \quad \text{for } t = \tau_0 + 1, \dots, k.$$

Consequently, the likelihood and its Hessian matrix are

$$\begin{aligned} \tilde{\ell}_k &= \sum_{t=\tau_0+1}^k I_t \log(a_t + b_t \phi_0 + c_t^T \theta) - (a_t + b_t \phi_0 + c_t^T \theta) \Lambda_j, \\ H_k &= - \sum_{t=\tau_0+1}^k \frac{I_t}{(a_t + b_t \phi_0 + c_t^T \theta)^2} \begin{pmatrix} b_t \\ c_t \end{pmatrix} \begin{pmatrix} b_t & c_t^T \end{pmatrix} \leq 0. \end{aligned}$$

Hence (7.1) is a global concave maximization problem.  $\blacksquare$ .

**Condition 3** When given  $\{(I_t, Z_t)\}_{1 \leq t \leq k}$ , consider the backward looking estimator in (A.1), for  $\varphi_t \triangleq \log(\tilde{R}_t) - \phi_0$ , there exist constants  $C_\varphi, C_{d\varphi}, C_{v\varphi}$ , such that, for  $1 \leq i \leq q$ ,

$$\max_{1 \leq t \leq k} |\varphi_t| \leq C_\varphi, \quad \max_{1 \leq t \leq k} \left| \frac{\partial \varphi_t}{\partial \theta_i} \right| \leq C_{d\varphi}, \quad \frac{1}{k^2} \sum_{\tau_0+1 \leq t < s \leq k} \left( \frac{\partial \varphi_t}{\partial \theta_i} - \frac{\partial \varphi_s}{\partial \theta_i} \right)^2 \geq C_{v\varphi}.$$

**Remark 0.1** Condition 3 is a restriction on  $\{Z_t\}_{t \geq 1}$  and it's loose consider the high variability this series of covariates have. In general, the condition is hard to verify despite been easily satisfied, an strict and sufficient alternative for the first two condition is to require  $\max_{k \geq \tau_0} \sum_{t=1}^k |Z_{k+1}^T H_k^{-1} (Z_t - \bar{Z}_k)| \leq (1 - \|\theta\|_1)/2$ , where  $H_k = \sum_{t=1}^k (Z_t - \bar{Z}_k)(Z_t - \bar{Z}_k)^T$ .

*Proof.(of Theorem 4.3)* We first eliminate the trivial cases where the pandemic cases vanishes or diverge to infinite, the first indicates the pandemic ends and the second is by nature unreasonable due to herd immunity or population limits. Thereby, without those two trivial cases, when given  $\{(I_t, Z_t)_{1 \leq t \leq k}\}$ , we have  $\max \Lambda_t$  is bounded from above by  $C_{u\lambda}$  and bounded away from zero by  $C_\lambda$ . Now, notice that  $\tilde{\beta}^{(k)}$  is essentially just a linear function of  $\theta$  and does not involve  $\phi_0$ , thereby, a simple reorganization of (4.3) leads to

$$\begin{aligned} \tilde{\ell}_k &\triangleq \sum_{t=\tau_0+1}^k \left( I_t \log \tilde{R}_t^{(k)} - \tilde{R}_t^{(k)} \Lambda_t \right) \\ &= \phi_0 \left( \sum_{t=\tau_0+1}^k I_t \right) - e^{\phi_0} \left( \sum_{t=\tau_0+1}^k e^{\sum_{i=1}^q \theta_i \log(\hat{R}_{t-i}^{(k-1)}) + Z_t^T \tilde{\beta}^{(k)}} \Lambda_t \right) \\ &\quad + \sum_{t=\tau_0+1}^k I_t \left( \sum_{i=1}^q \theta_i \log(\hat{R}_{t-i}^{(k-1)}) + Z_t^T \tilde{\beta}^{(k)} \right), \end{aligned}$$

Notice that

$$\frac{\partial^2 \tilde{\ell}_k}{(\partial \phi_0)^2} = -e^{\phi_0} \left( \sum_{t=\tau_0+1}^k e^{\sum_{i=1}^q \theta_i \log(\hat{R}_{t-i}^{(k-1)}) + Z_t^T \tilde{\beta}^{(k)}} \Lambda_t \right) \leq 0,$$

so by letting  $\partial \tilde{\ell}_k / \partial \phi_0 = 0$ , we have  $(\hat{\phi}_0^{(k)}, \hat{\theta}^{(k)})$  satisfy the equations

$$\begin{aligned} \exp(\phi_0) &= \left( \sum_{t=\tau_0+1}^k I_t \right) \cdot \left( \sum_{t=\tau_0+1}^k e^{\sum_{i=1}^q \theta_i \log(\hat{R}_{t-i}^{(k-1)}) + Z_t^T \tilde{\beta}^{(k)}} \Lambda_t \right)^{-1}, \\ \hat{\theta}^{(k)} &= \arg \max_{\|\theta\|_1 \leq 1} \left[ \sum_{t=\tau_0+1}^k I_t \left( \sum_{i=1}^q \theta_i \log(\hat{R}_{t-i}^{(k-1)}) + Z_t^T \tilde{\beta}^{(k)} \right) \right. \\ &\quad \left. - \left( \sum_{t=\tau_0+1}^k I_t \right) \log \left( \sum_{t=\tau_0+1}^k e^{\sum_{i=1}^q \theta_i \log(\hat{R}_{t-i}^{(k-1)}) + Z_t^T \tilde{\beta}^{(k)}} \Lambda_t \right) \right] \triangleq \arg \max_{\|\theta\|_1 \leq 1} \tilde{\ell}_{\theta, k}, \quad (\text{C.1}) \end{aligned}$$

or equivalently, plug the form of optimal  $\phi_0$  into the quasi-score estimating equation and conclude  $\hat{\theta}^{(k)}$  satisfy  $\partial\tilde{\ell}_{\theta,k}/\partial\theta = 0$ , i.e.,

$$0 = -\left(\sum_{t=\tau_0+1}^k I_t\right) \frac{\sum_{t=\tau_0+1}^k e^{\varphi_t^{(k)}} \Lambda_t \frac{\partial \varphi_t^{(k)}}{\partial \theta}}{\sum_{t=\tau_0+1}^k e^{\varphi_t^{(k)}} \Lambda_t} \Big|_{\theta=\hat{\theta}^{(k)}} + \sum_{t=\tau_0+1}^k I_t \frac{\partial \varphi_t^{(k)}}{\partial \theta}, \quad (\text{C.2})$$

where  $\varphi_t^{(k)} = \sum_{i=1}^q \theta_i \log(\hat{R}_{t-i}^{(k-1)}) + Z_t^T \tilde{\beta}^{(k)}$ , and for  $1 \leq i \leq q$ ,

$$\frac{\partial \varphi_t^{(k)}}{\partial \theta_i} = \log(\hat{R}_{t-i}^{(k-1)}) + Z_t^T \frac{\partial \tilde{\beta}^{(k)}}{\partial \theta_i}, \quad \frac{\partial^2 \varphi_t^{(k)}}{\partial \theta \partial \theta^T} = 0.$$

Meanwhile, Cauchy's inequality shows that for each  $k \geq \tau_0 + 1$ ,

$$\begin{aligned} & \left( \sum_{t=\tau_0+1}^k e^{\varphi_t^{(k)}} \Lambda_t \right)^2 \frac{\partial^2 \tilde{\ell}_{\theta,k}}{\partial \theta \partial \theta^T} \Big/ \left( \sum_{t=\tau_0+1}^k I_t \right) \\ &= - \left[ \sum_{t=\tau_0+1}^k e^{\varphi_t^{(k)}} \Lambda_t \left( \frac{\partial \varphi_t^{(k)}}{\partial \theta} \right) \left( \frac{\partial \varphi_t^{(k)}}{\partial \theta} \right)^T \right] \left( \sum_{t=\tau_0+1}^k e^{\varphi_t^{(k)}} \Lambda_t \right) \\ & \quad + \left[ \sum_{t=\tau_0+1}^k e^{\varphi_t^{(k)}} \Lambda_t \left( \frac{\partial \varphi_t^{(k)}}{\partial \theta} \right) \right] \left[ \sum_{t=\tau_0+1}^k e^{\varphi_t^{(k)}} \Lambda_t \left( \frac{\partial \varphi_t^{(k)}}{\partial \theta} \right) \right]^T \leq 0, \end{aligned} \quad (\text{C.3})$$

thereby the solution of

$$\hat{\theta}^{(k)} \triangleq \arg \max_{\|\theta\|_1 < 1} \tilde{\ell}_{\theta,k}, \quad (\text{C.4})$$

would be a unique point or a closed interval. The second case happens only when the equality sign of (C.3) holds, i.e.,

$$\frac{\partial \varphi_t^{(k)}}{\partial \theta} = C_0, \quad t = \tau_0 + 1, \dots, k,$$

for some constant  $C_0$ . This implies the quasi-score equation (C.2) holds for all  $\theta \in \{\|\theta\|_1 < 1\}$ , for instance the case where  $\theta = 0$ , which is trivial since (3.3) degenerate to linear regression and we omit discussions on this scenario. On the contrast, we have  $\hat{\theta}^{(k)}$  is the unique solution of (C.2) and  $\hat{\theta}^{(k-1)}$  satisfy the same equation with  $k$  replaced by  $k-1$ , i.e.,

$$0 = \sum_{t=\tau_0+1}^{k-1} I_t \frac{\partial \varphi_t^{(k-1)}}{\partial \theta} - \left( \sum_{t=\tau_0+1}^{k-1} I_t \right) \frac{\sum_{t=\tau_0+1}^{k-1} e^{\varphi_t^{(k-1)}} \Lambda_t \frac{\partial \varphi_t^{(k-1)}}{\partial \theta}}{\sum_{t=\tau_0+1}^{k-1} e^{\varphi_t^{(k-1)}} \Lambda_t}. \quad (\text{C.5})$$

Recall (A.1) and combine (C.2) and (C.5) leads to

$$\begin{aligned} & \left( \sum_{t=\tau_0+1}^k I_t \right) \frac{\sum_{t=\tau_0+1}^k e^{\varphi_t^{(k)}} \Lambda_t \frac{\partial \varphi_t^{(k)}}{\partial \theta}}{\sum_{t=\tau_0+1}^k e^{\varphi_t^{(k)}} \Lambda_t} \Big|_{\theta=\hat{\theta}^{(k)}} = \sum_{t=\tau_0+1}^k I_t \frac{\partial \varphi_t^{(k)}}{\partial \theta} \\ & = \left( \sum_{t=\tau_0+1}^{k-1} I_t \right) \frac{\sum_{t=\tau_0+1}^{k-1} e^{\varphi_t^{(k-1)}} \Lambda_t \frac{\partial \varphi_t^{(k-1)}}{\partial \theta}}{\sum_{t=\tau_0+1}^{k-1} e^{\varphi_t^{(k-1)}} \Lambda_t} \Big|_{\theta=\hat{\theta}^{(k-1)}} + I_k \frac{\partial \varphi_k^{(k)}}{\partial \theta}, \end{aligned}$$

hence

$$\begin{aligned} & \left( \sum_{t=\tau_0+1}^k I_t \right) \frac{\sum_{t=\tau_0+1}^k e^{\varphi_t^{(k)}} \Lambda_t \frac{\partial \varphi_t^{(k)}}{\partial \theta}}{\sum_{t=\tau_0+1}^k e^{\varphi_t^{(k)}} \Lambda_t} \Big|_{\theta=\hat{\theta}^{(k)}} \\ & - \left( \sum_{t=\tau_0+1}^{k-1} I_t \right) \frac{\sum_{t=\tau_0+1}^{k-1} e^{\varphi_t^{(k-1)}} \Lambda_t \frac{\partial \varphi_t^{(k-1)}}{\partial \theta}}{\sum_{t=\tau_0+1}^{k-1} e^{\varphi_t^{(k-1)}} \Lambda_t} \Big|_{\theta=\hat{\theta}^{(k)}} - I_k \frac{\partial \varphi_k^{(k)}}{\partial \theta} \\ & = \left( \sum_{t=\tau_0+1}^{k-1} I_t \right) \frac{\sum_{t=\tau_0+1}^{k-1} e^{\varphi_t^{(k-1)}} \Lambda_t \frac{\partial \varphi_t^{(k-1)}}{\partial \theta}}{\sum_{t=\tau_0+1}^{k-1} e^{\varphi_t^{(k-1)}} \Lambda_t} \Big|_{\theta=\hat{\theta}^{(k-1)}} - \left( \sum_{t=\tau_0+1}^{k-1} I_t \right) \frac{\sum_{t=\tau_0+1}^{k-1} e^{\varphi_t^{(k-1)}} \Lambda_t \frac{\partial \varphi_t^{(k-1)}}{\partial \theta}}{\sum_{t=\tau_0+1}^{k-1} e^{\varphi_t^{(k-1)}} \Lambda_t} \Big|_{\theta=\hat{\theta}^{(k)}}, \end{aligned}$$

and it further implies

$$\begin{aligned} & \frac{\partial^2 \tilde{\ell}_{\theta, k-1}}{\partial \theta \partial \theta^T} \Big|_{\theta=\theta^*} \cdot (\hat{\theta}^{(k)} - \hat{\theta}^{(k-1)}) \\ & = \left( \sum_{t=\tau_0+1}^{k-1} I_t \right) \left[ \frac{e^{\varphi_k^{(k)}} \Lambda_k \frac{\partial \varphi_k^{(k)}}{\partial \theta} + \sum_{t=\tau_0+1}^{k-1} e^{\varphi_t^{(k)}} \Lambda_t \frac{\partial \varphi_t^{(k)}}{\partial \theta}}{e^{\varphi_k^{(k)}} \Lambda_k + \sum_{t=\tau_0+1}^{k-1} e^{\varphi_t^{(k)}} \Lambda_t} - \frac{\sum_{t=\tau_0+1}^{k-1} e^{\varphi_t^{(k-1)}} \Lambda_t \frac{\partial \varphi_t^{(k-1)}}{\partial \theta}}{\sum_{t=\tau_0+1}^{k-1} e^{\varphi_t^{(k-1)}} \Lambda_{k-1}} \right] \Big|_{\theta=\hat{\theta}^{(k)}} \\ & + I_k \left[ \frac{\sum_{t=\tau_0+1}^k e^{\varphi_t^{(k)}} \Lambda_t \frac{\partial \varphi_t^{(k)}}{\partial \theta}}{\sum_{t=\tau_0+1}^k e^{\varphi_t^{(k)}} \Lambda_t} \Big|_{\theta=\hat{\theta}^{(k)}} - \frac{\partial \varphi_k^{(k)}}{\partial \theta} \right] \end{aligned} \quad (\text{C.6})$$

for some  $\theta^*$  between  $\hat{\theta}^{(k-1)}$  and  $\hat{\theta}^{(k)}$ . Since  $\psi_t$  is actually invariant over  $k \geq t$ , so

$$\begin{aligned} & \left[ \frac{\sum_{t=\tau_0+1}^k e^{\varphi_t^{(k)}} \Lambda_t \frac{\partial \varphi_t^{(k)}}{\partial \theta}}{\sum_{t=\tau_0+1}^k e^{\varphi_t^{(k)}} \Lambda_t} - \frac{\sum_{t=\tau_0+1}^{k-1} e^{\varphi_t^{(k-1)}} \Lambda_t \frac{\partial \varphi_t^{(k-1)}}{\partial \theta}}{\sum_{t=\tau_0+1}^{k-1} e^{\varphi_t^{(k-1)}} \Lambda_{k-1}} \right] \Big|_{\theta=\hat{\theta}^{(k)}} \\ & = \frac{\sum_{t=\tau_0+1}^{k-1} e^{\varphi_k} \Lambda_k e^{\varphi_t} \Lambda_t \left( \frac{\partial \varphi_k}{\partial \theta} - \frac{\partial \varphi_t}{\partial \theta} \right)}{\left( \sum_{t=\tau_0+1}^k e^{\varphi_t^{(k)}} \Lambda_t \right) \left( \sum_{s=\tau_0+1}^{k-1} e^{\varphi_s^{(k-1)}} \Lambda_s \right)} \Big|_{\theta=\hat{\theta}^{(k)}} = O\left(\frac{1}{k}\right) \end{aligned} \quad (\text{C.7})$$

By condition 3, and for each  $1 \leq i \leq q$ , we have

$$\begin{aligned}
& \left| \frac{\partial^2 \tilde{\ell}_{\theta, k-1}}{(\partial \theta_i)^2} \right|_{\theta=\theta^*} \left/ \left( \sum_{t=\tau_0+1}^{k-1} I_t \right) \right. \\
&= \frac{\left( \sum_{t=\tau_0+1}^{k-1} e^{\varphi_t^{(k-1)}} \Lambda_t \left( \frac{\partial \varphi_t^{(k-1)}}{\partial \theta_i} \right)^2 \right) \left( \sum_{t=\tau_0+1}^{k-1} e^{\varphi_t^{(k-1)}} \Lambda_t \right)}{\left( \sum_{t=\tau_0+1}^{k-1} e^{\varphi_t^{(k-1)}} \Lambda_t \right)^2} - \frac{\left( \sum_{t=\tau_0+1}^{k-1} e^{\varphi_t^{(k-1)}} \Lambda_t \left( \frac{\partial \varphi_t^{(k-1)}}{\partial \theta_i} \right) \right)^2}{\left( \sum_{t=\tau_0+1}^{k-1} e^{\varphi_t^{(k-1)}} \Lambda_t \right)^2} \\
&= \frac{\sum_{\tau_0+1 \leq t < s \leq k-1} e^{\varphi_t^{(k-1)} + \varphi_s^{(k-1)}} \Lambda_t \Lambda_s \left( \frac{\partial \varphi_t^{(k-1)}}{\partial \theta_i} - \frac{\partial \varphi_s^{(k-1)}}{\partial \theta_i} \right)^2}{\left( \sum_{t=\tau_0+1}^{k-1} e^{\varphi_t^{(k-1)}} \Lambda_t \right)^2} \geq e^{-4C_\varphi} \frac{C_\lambda^2}{C_{u\lambda}^2} C_{v\varphi}.
\end{aligned}$$

Combine with (C.6) and (C.7) implies that

$$|\hat{\theta}_i^{(k)} - \hat{\theta}_i^{(k-1)}| = O\left(\frac{1}{k} + \frac{I_k}{\left(\sum_{t=\tau_0+1}^{k-1} I_t\right)}\right).$$

■.

When consider the forward-looking estimator, it behaves much more complicated, first, a stronger condition would be needed just to conclude a similar result, for instance,

**Condition 4** Suppose  $\|\theta\|_1 < \phi < 1$ ,  $\max \|Z_t\|_1 \leq M$ , and when given  $\{(I_t, Z_t)\}_{1 \leq t \leq k}$ , for  $\varphi_t^{(k)} \triangleq \log(\tilde{R}_t^{(k)}) - \phi_0$ , there exist constants  $C_\varphi, C_{d\varphi}, C_{v\varphi}$ , s.t., for  $1 \leq i \leq q$ , and each  $k$ ,

$$\max_{1 \leq t \leq k} |\varphi_t^{(k)}| \leq C_\varphi, \quad \max_{1 \leq t \leq k} \left| \frac{\partial \varphi_t^{(k)}}{\partial \theta_i} \right| \leq C_{d\varphi}, \quad \frac{1}{k^2} \sum_{\tau_0+1 \leq t < s \leq k} \left( \frac{\partial \varphi_t^{(k)}}{\partial \theta_i} - \frac{\partial \varphi_s^{(k)}}{\partial \theta_i} \right)^2 \geq C_{v\varphi}.$$

Second, the proof of Theorem 4.3 needs justification from line to line. Since now  $\varphi_t^{(k)}$  is a term involve  $k$ , so we define  $d_{\varphi_t}^{(k)} = |\hat{\varphi}_t^{(k)} - \hat{\varphi}_t^{(k-1)}|$  and similarly define  $d_\theta^{(k)} = \|\theta^{(k)} - \theta^{(k-1)}\|_1$ . Since  $\varphi_t^{(k)}$  is bounded uniformly over  $k$ , so we have  $|e^{\varphi_t^{(k)}} - e^{\varphi_t^{(k)}}| \leq O(d_{\varphi_t}^{(k)})$ . Consequently,

(C.7) for forward-looking estimator should be justified to

$$\begin{aligned}
& \left[ \frac{\sum_{t=\tau_0+1}^k e^{\varphi_t^{(k)}} \Lambda_t \frac{\partial \varphi_t^{(k)}}{\partial \theta}}{\sum_{t=\tau_0+1}^k e^{\varphi_t^{(k)}} \Lambda_t} - \frac{\sum_{t=\tau_0+1}^{k-1} e^{\varphi_t^{(k-1)}} \Lambda_t \frac{\partial \varphi_t^{(k-1)}}{\partial \theta}}{\sum_{t=\tau_0+1}^{k-1} e^{\varphi_t^{(k-1)}} \Lambda_{k-1}} \right] \Big|_{\theta=\hat{\theta}^{(k)}} \\
& \leq O\left(\frac{1}{k}\right) + \max_t \frac{\partial d_{\varphi_t}^{(k)}}{\partial \theta} + \frac{\sum_{t=\tau_0+1}^{k-1} \sum_{s=\tau_0+1}^{k-1} \frac{\partial \varphi_t^{(k-1)}}{\partial \theta} \Lambda_t \Lambda_s (\exp(\varphi_t^{(k)} + \varphi_s^{(k-1)}) - \exp(\varphi_t^{(k-1)} + \varphi_s^{(k)}))}{\left(\sum_{t=\tau_0+1}^{k-1} e^{\varphi_t^{(k)}} \Lambda_t\right) \left(\sum_{s=\tau_0+1}^{k-1} e^{\varphi_s^{(k-1)}} \Lambda_s\right)} \Big|_{\theta=\hat{\theta}^{(k)}} \\
& \leq O\left(\frac{1}{k}\right) + \max_t \frac{\partial d_{\varphi_t}^{(k)}}{\partial \theta} + O\left(\max_t d_{\varphi_t}^{(k)}\right)
\end{aligned}$$

Accordingly, we have

$$d_{\theta}^{(k)} \leq O\left(\frac{1}{k} + \frac{I_k}{\left(\sum_{t=\tau_0+1}^{k-1} I_t\right)} + \max_t \frac{\partial d_{\varphi_t}^{(k)}}{\partial \theta} + \max_t d_{\varphi_t}^{(k)}\right).$$

## References

Atchadé, Y. F. (2009), ‘A strong law of large numbers for martingale arrays’, *arXiv preprint arXiv:0905.2761* .

Chen, Y.-C., Lu, P.-E. and Chang, C.-S. (2020), ‘A time-dependent sir model for covid-19’, *arXiv preprint arXiv:2003.00122* .

Chiou, J.-M. and Müller, H.-G. (1998), ‘Quasi-likelihood regression with unknown link and variance functions’, *Journal of the American Statistical Association* **93**(444), 1376–1387.

Fan, J. and Gijbels, I. (1996), *Local polynomial modelling and its applications: monographs on statistics and applied probability 66*, Vol. 66, CRC Press.

Friedman, J. H. (1991), ‘Multivariate adaptive regression splines’, *The annals of statistics* pp. 1–67.

Ghosal, S. and Chandra, T. K. (1998), ‘Complete convergence of martingale arrays’, *Journal of Theoretical Probability* **11**(3), 621–631.

Hall, P. and Heyde, C. C. (2014), *Martingale limit theory and its application*, Academic press.

Hall, P., Turlach, B. A. et al. (1997), ‘Interpolation methods for nonlinear wavelet regression with irregularly spaced design’, *The Annals of Statistics* **25**(5), 1912–1925.

Kaufmann, H. (1987), ‘Regression models for nonstationary categorical time series: asymptotic estimation theory’, *The Annals of Statistics* pp. 79–98.

Li, Q., Guan, X., Wu, P., Wang, X., Zhou, L., Tong, Y., Ren, R., Leung, K. S., Lau, E. H., Wong, J. Y. et al. (2020), ‘Early transmission dynamics in wuhan, china, of novel coronavirus–infected pneumonia’, *New England journal of medicine* .

Liang, K.-Y. and Hanfelt, J. (1994), ‘On the use of the quasi-likelihood method in teratological experiments’, *Biometrics* pp. 872–880.

Lipsitch, M., Joshi, K. and Cobey, S. E. (2020), ‘Comment on pan a, liu l, wang c, et al.,” association of public health interventions with the epidemiology of the covid-19 outbreak in wuhan, china,” jama, published online april 10, 2020’.

Pratt, J. W. (1960), ‘On interchanging limits and integrals’, *The Annals of Mathematical Statistics* **31**(1), 74–77.

Quick, C., Dey, R. and Lin, X. (2021), ‘Regression models for understanding covid-19 epidemic dynamics with incomplete data’, *Journal of the American Statistical Association* **116**(536), 1561–1577.

The New York Times, J. t. (2020, July 28th), ‘See how all 50 states are reopening (and closing again)’.

**URL:** [nytimes.com/interactive/2020/us/states-reopen-map-coronavirus.html](https://nytimes.com/interactive/2020/us/states-reopen-map-coronavirus.html)

Unacast (2021, July 1st), ‘Social distancing scoreboard’.

**URL:** <https://www.unacast.com/covid19/socialdistancing-scoreboard#methodology>